Relativistic EOM-CCSD for core-excited and core-ionized state energies based on the 4-component Dirac-Coulomb(-Gaunt) Hamiltonian

Loïc Halbert, Marta López Vidal, Avijit Shee, Sonia Coriani, André Severo Pereira Gomes

JCTC Journal of Chemical Theory and Computation

pubs.acs.org/JCTC Article

Relativistic EOM-CCSD for Core-Excited and Core-Ionized State Energies Based on the Four-Component Dirac−Coulomb(−Gaunt) Hamiltonian

Loïc Halbert,* Marta L. Vidal,* Avijit Shee,* Sonia Coriani,* and André Severo Pereira Gomes*

Cite This: *J. Chem. Theory Comput.* 2021, 17, 3583−3598 Read Online

ACCESS | Metrics & More | Article Recommendations | Supporting Information

ABSTRACT: We report an implementation of the core−valence separation approach to the four-component relativistic Hamiltonian-based equation-of-motion coupled-cluster with singles and doubles theory (CVS-EOM-CCSD) for the calculation of relativistic core-ionization potentials and core-excitation energies. With this implementation, which is capable of exploiting double group symmetry, we investigate the effects of the different CVS-EOM-CCSD variants and the use of different Hamiltonians based on the exact two-component (X2C) framework on the energies of different core-ionized and -excited states in halogen- (CH_3I, HX, and X^-, X = Cl−At) and xenon-containing (Xe, XeF_2) species. Our results show that the X2C molecular mean-field approach [Sikkema, J.; et al. *J. Chem. Phys.* **2009**, *131*, 124116], based on four-component Dirac−Coulomb mean-field calculations ($^2DC^M$), is capable of providing core excitations and ionization energies that are nearly indistinguishable from the reference four-component energies for up to and including fifth-row elements. We observe that two-electron integrals over the small-component basis sets lead to non-negligible contributions to core binding energies for the K and L edges for atoms such as iodine or astatine and that the approach based on Dirac−Coulomb−Gaunt mean-field calculations ($^2DCG^M$) are significantly more accurate than X2C calculations for which screened two-electron spin−orbit interactions are included via atomic mean-field integrals.

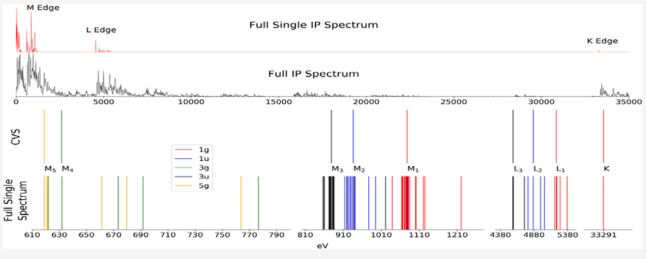

1. INTRODUCTION

X-ray spectroscopies, which typically probe core electrons through electronic excitation or ionization, are particularly suitable techniques to study the local environment of atoms, molecules, and materials, as the localized nature of the core orbitals makes them very selective and sensitive.[1,2]

Over the last few years, new X-ray free-electron lasers (XFEL) and last-generation synchrotrons have started operating. These advanced light sources have opened the door to a variety of new X-ray-based spectroscopies,[3−5] including those operating in time-resolved and nonlinear regimes.[2−6] As stated, for instance, by Milne, Penfold, and Chergui in their review:[7] "[...] The progress of experimental techniques for core level spectroscopies is unraveling subtle spectral features implying that high-level theoretical approaches are required to interpret them [...]". The experimental X-ray spectra need to be compared to highly accurate theoretical calculations to assign spectral features and to relate experimental measurements to the structure and dynamic properties of the probed molecular system.

Among the methods, one can use to calculate core binding energies ΔSCF,[8,9] which stands out due to the combination of low-computational cost and good results. By performing separate self-consistent field (SCF) calculations on the original (generally neutral and closed-shell) and ionized (generally open-shell) species, it introduces the important orbital relaxation that accompanies the creation of the core hole, though at the expense of requiring several calculations for the edges of interest and with the potential complication that the required open-shell calculations may be difficult to converge. The same approach can be applied in a straightforward manner to density functional theory (DFT),[10] with the additional complication that it will show a certain dependence on the chosen density functional. The same idea of performing separate calculations for the initial and the target states can be used to devise approaches based on correlated wave functions such as MP2[11] or coupled-cluster (CC).[12,13] Analogous methods for core excitations have also been formulated,[14−22] though this has proven somewhat more cumbersome than for ionizations, since one has to select orbital pairs that should represent the transitions and converge such excited configurations. In a number of these approaches, the orbitals for the ground and excited/ionized states are not orthogonal, making, for instance, the calculation of transition moments more involved.

Received: November 18, 2020
Published: May 4, 2021

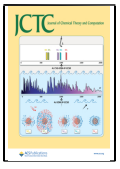

The above difficulties are circumvented with approaches that diagonalize the same Hamiltonian for both the original and the ionized or excited states. As such, the excited-state approaches based on wave function theory, like, for instance, (multireference) configuration interaction (MRCI),[23−26] equation-of-motion CC (EOM-CC)[27−35] and multireference (EOM)-CC,[26,36] and linear response complete active space SCF (LR-CASSCF),[37] Green's functions such as the algebraic diagrammatic construction (ADC),[38−41] or time-dependent density functional theory (TDDFT),[10,42,43] can all be used to target core-excited or ionized states. One downside is, however, that now relaxation has to be accounted for by the correlated electronic structure approach. Among these, single-reference CC methods and in particular those based on EOM and the closely related linear response (LRCC) formalisms[44−50] are capable of treating electron correlation accurately and in a balanced way between the ground and excited states, including a good deal of relaxation effects, and have an appealing "black box" nature (though they are less adept than MRCI/multireference coupled cluster (MRCC) at treating cases for which the ground state shows a strong multireference nature).

Irrespective of the correlated method, a particular difficulty for determining core states by diagonalizing a many-body Hamiltonian is that such states appear at high energies, where spectra are potentially very dense (see for example Figure 2). Thus, a naive application of procedures, which target exterior roots (such as the Davidson algorithm), would require for solving a very large number of roots. One way to overcome this issue is through the use of methods capable of solving interior roots without requiring that all of them are targeted, as those recently devised and applied to multiconfigurational,[37] EOM-CC,[32,51] and mean-field[52,53] wave functions.

A more widespread strategy,[23,28,29,31,34,35,37−40,54−57] which we follow in this paper, is to employ physically motivated approximations to the original Hamiltonian, in particular within the core−valence separation (CVS) approximation.[58] The core−valence separation is justified by the large spatial and energetic separation between the valence and core orbitals/electrons. On the one hand, CVS allows to straightforwardly address the highly energetic core states with minor modifications to pre-existing eigenvalue solvers. On the other hand, the CVS helps alleviating convergence issues due to a large number of valence ionized states in the frequency region of the core excitations, which is particularly afflicting methods that explicitly include double excitations in their parametrization.[59,60] One can also regard the core states as metastable Feshbach resonances embedded in the (valence) ionization continuum, and the application of CVS helps stabilizing them. Further details on the CVS approach will be given in Section 2.3.

A second issue to be addressed for core states is the importance of relativistic effects,[61−63] which significantly alter the energies of inner electrons, and consequently, the core spectra of atoms and molecules: due to the high velocities of their electrons (a significant fraction of the speed of light), core s and p orbitals contract (with an associated lowering of their orbital energies), while due to increased screening, d and f orbitals expand (with an associated increase in their orbital energies). At the same time, orbitals that are degenerate in a nonrelativistic framework (p, d, f) are (strongly) split due to spin−orbit coupling, and particularly so for the innermost orbitals.

Relativistic effects are so pronounced in the core region that, even for molecules containing only elements of the first and second rows, they are very important for the accurate determination of K and L edge spectra. While rather approximate treatments of relativistic effects can yield accurate results for light elements,[12,64−67] a more consistent way of treating these effects is through an electronic Hamiltonian based on the four-component Dirac operator, as it is accurate all the way down to the heaviest elements (5d and 6d transition metals, lanthanides, and actinides). As such, four-component-based methods are ideally suited to treat the core spectra across the periodic table and to probe K, L, and M edges of heavy elements,[11,68,69] which are much more complex to interpret than those of lighter elements. Though the availability of efficient implementations[70−72] has in recent years enabled mean-field four-component calculation for large-scale applications, the additional basis sets required to represent the small-component part of the molecular spinors still place a considerable burden on such calculations compared to the nonrelativistic case.

An important development to overcome such issues has been the introduction of the so-called exact two-component (X2C) methods,[73−79] in which a transformation to decouple the positive and negative-energy states of the Dirac Hamiltonian is available in the matrix form and, unlike its more approximate counterparts, yields exactly the same positive energy spectrum as the original four-component Hamiltonian. We refer the reader to a recent comprehensive review on the relativistic electronic structure for more details.[63]

We note that among the different X2C variants, those that construct the transformation matrix on the basis of converged four-component atomic or molecular mean-field calculations[75,77,79] are particularly interesting to correlated calculations[79−83] since they avoid the handling of two-electron integrals over small-component basis functions in the transformation into molecular spinors, while largely avoiding errors with respect to the original four-component Hamiltonian on the description of two-electron spin−orbit coupling contributions, compared to approaches in which the decoupling is performed based on the one-electron Dirac Hamiltonian prior to the mean-field step.[76]

In this study, we present an approach to study core ionization (and excitation) through the use of projectors, inspired by the work of Coriani and Koch[28,29] but extended to the four-component EOM-CCSD approach developed by Shee et al.[84] in the DIRAC relativistic electronic structure package.[85] Because of the availability of different Hamiltonians in DIRAC, we also investigate the performance of two-component approaches[79] with respect to the four-component one. We refer to, e.g., refs 86−101 for other examples of relativistic EOM-CC implementations, and to refs 12, 31, 34, 35, 55, 59, 60, 65, 102, 103 for other examples of CVS-EOM-CC implementations. We also wish to underline that the literature on the theoretical approaches for core spectroscopy is vast and rapidly increasing, and the studies cited in the previous paragraphs cannot be considered exhaustive. We refer the reader to a number of recent review papers for more thorough accounts.[2,24,43,104]

The paper is organized as follows. In Section 2, we give a brief outline of EOM-CCSD (Section 2.1) and of CVS (Section 2.2), as well as the details of the current implementation (Section 2.3). In Section 3, we provide the computational details of the calculations. In Section 4, we present the results obtained with the newly implemented method, where we discuss the accuracy of the CVS approximation (Section 4.1), the performance of the different CVS variants (Section 4.2), the influence of the Hamiltonian (Section 4.3), and the comparison to experiment

https://doi.org/10.1021/acs.jctc.0c01203
J. Chem. Theory Comput. 2021, 17, 3583−3598

for ionization (Section 4.4) and excitation (Section 4.5) energies. Finally, Section 5 summarizes our conclusions.

2. METHODS AND IMPLEMENTATION

In what follows, indices (i, j, k, l), (a, b, c, d), and (p, q, r, s) refer to occupied, virtual, and general orbitals, respectively.

2.1. EOM-CC. In EOM-CC, the ground state is treated at the coupled-cluster level. Its eigenfunction is hence given by the exponential ansatz

$$|\Psi_{CC}\rangle = e^{\hat{T}}|\Phi_0\rangle; \quad \hat{T} = \sum_{\mu} t_\mu \hat{\tau}_\mu \tag{1}$$

where Φ_0 is the reference (typically Hartree−Fock) determinant and the operator $\hat{T}$ is the cluster operator. Truncating $\hat{T}$ to single (S) and double (D) excitations yields the coupled-cluster singles-and-doubles (CCSD) model

$$\hat{T} = \hat{T}_1 + \hat{T}_2; \quad \hat{T}_1 = \sum_{ia} t_i^a a_a^\dagger a_i; \quad \hat{T}_2 = \frac{1}{4}\sum_{ijab} t_{ij}^{ab} a_a^\dagger a_b^\dagger a_j a_i \tag{2}$$

The energy and the cluster amplitudes are found from the CC equations

$$\langle \Phi_0|\widehat{\bar{H}}|\Phi_0\rangle = E \tag{3}$$

$$\langle \Phi_\mu|\widehat{\bar{H}}|\Phi_0\rangle = 0; \quad |\Phi_\mu\rangle = \hat{\tau}_\mu|\Phi_0\rangle \tag{4}$$

where the similarity-transformed Hamiltonian $\widehat{\bar{H}}$ has been defined as

$$\widehat{\bar{H}} \equiv e^{-\hat{T}}\hat{H}e^{\hat{T}} \tag{5}$$

In the equation-of-motion coupled-cluster (EOM-CC) method,[44,47] the target states are obtained by the diagonalization of the non-Hermitian similarity-transformed Hamiltonian. This non-Hermicity gives rise to right (R) and left (L) eigenvectors that are not adjoints of each other, obtained solving two different eigenvalue equations

$$\widehat{\bar{H}}|R_\mu\rangle = E_\mu|R_\mu\rangle \tag{6}$$

$$\langle L_\mu|\widehat{\bar{H}} = E_\mu\langle L_\mu| \tag{7}$$

for a given excited state μ with energy E_μ, where the eigenstates are chosen to satisfy the biorthogonality conditions

$$\langle L_\mu|R_\nu\rangle = \delta_{\mu\nu} \tag{8}$$

Right and left wave functions of the target states have been thus obtained from a linear parametrization of the reference state through the $\hat{R}$ or $\hat{L}$ operators

$$|\Psi_\mu\rangle = e^{\hat{T}}\hat{R}_\mu|\Phi_0\rangle \tag{9}$$

and

$$\langle\bar{\Psi}_\mu| = \langle\Phi_0|\hat{L}_\mu e^{-\hat{T}} \tag{10}$$

Therefore, the choice of the $\hat{R}$ and $\hat{L}$ operators defines which target states to study, yielding different EOM-CC models. In the present work, we focus on the models for electronically excited (EE) states and ionization potentials (IP)

- EOM-CCSD-EE

$$\hat{R}^{EE} = r_0 + \sum_{ia} r_i^a\{a_a^\dagger a_i\} + \sum_{i>j,a>b} r_{ij}^{ab}\{a_a^\dagger a_b^\dagger a_j a_i\} \tag{11}$$

$$\hat{L}^{EE} = l_0 + \sum_{ia} l_a^i\{a_i^\dagger a_a\} + \sum_{i>j,a>b} l_{ab}^{ij}\{a_i^\dagger a_j^\dagger a_b a_a\} \tag{12}$$

- EOM-CCSD-IP

$$\hat{R}^{IP} = \sum_{i} r_i\{a_i\} + \sum_{i>j,a} r_{ij}^a\{a_a^\dagger a_j a_i\} \tag{13}$$

$$\hat{L}^{IP} = \sum_{i} l^i\{a_i^\dagger\} + \sum_{i>j,a} l_a^{ij}\{a_j^\dagger a_i^\dagger a_a\} \tag{14}$$

where curly brackets refer to normal ordering with respect to the Fermi vacuum defined by the reference Φ_0 and the sets $\{\boldsymbol{r}\}$, $\{\boldsymbol{l}\}$ to the amplitudes of the corresponding operators.

We have here truncated our $\hat{R}$ and $\hat{L}$ operators at the singles-doubles level since the same truncation is used for the $\hat{T}$ operators.

2.2. Core−Valence Separation Approximation. The essence of the core−valence separation (CVS) approximation[58] is to decouple valence and core electrons based on their difference in energy and spatial extension. This allows solving the regular, in this case, EOM-CC equations only in the space of the relevant orbitals. However, different flavors of CVS exist, which introduce different levels of approximation. Coriani and Koch first introduced the CVS approximation within coupled-cluster theory[28,29] by applying a projector that zeroes out the amplitudes of all excitations that do not involve at least one core electron. Recently, the frozen-core (FC) CVS-EOM-CCSD approach has been proposed that introduces a further approximation, in this case at the ground-state level: the core orbitals are frozen when solving the CC equations for the ground state, whereas they are the only active ones when solving the EOM equations. Both schemes retain the contribution from excitations simultaneously involving two core orbitals. However, these excitations are located in a much higher range of energy in the spectrum and might therefore also be decoupled. This is the strategy adopted, for instance, by Dreuw and co-workers in their implementation of the CVS within the ADC family of methods.[39,40,105]

In this work, the CVS implementation has been carried out following the recipe proposed by Coriani and Koch:[28] a projector P is applied at each iteration of the Davidson procedure during the resolution of the EOM-CC equations. This projector P selectively zeroes out the unwanted contributions to the EOM trial/solution vectors according to the approximation used. In the CVS approach, unwanted contributions generally correspond to excited determinants involving only occupied valence (v) spinors. In the case of EOM-EE, the application of a projector $P \equiv P^{CVS}$ to a target electronic state $|\Psi_\mu^{EE}\rangle$ corresponds to

$$P^{CVS}|\Psi_\mu^{EE}\rangle \Rightarrow {}^\mu r_i^a = {}^\mu r_{ij}^{ab} = 0 \text{ if } i, j \in v \tag{15}$$

though one can also devise variants in which additional contributions are zeroed out, see Section 2.3 for details. With this definition, the eigenvalue equation to be solved to get the energy of the target states becomes

$$P^{CVS}(\widehat{\bar{H}}P^{CVS}|R_\mu\rangle) = E_\mu P^{CVS}|R_\mu\rangle \tag{16}$$

https://doi.org/10.1021/acs.jctc.0c01203
J. Chem. Theory Comput. 2021, 17, 3583−3598

It should be noted that the projection scheme does not yield any savings, in terms of memory usage or operations. Some of us[31] have recently gone beyond the use of projection operators and introduced an analytical formulation of CVS, in which only the sub-blocks of the similarity-transformed Hamiltonian that are relevant to the calculation of a given core level are actually formed, thus resulting in a more efficient implementation. This formulation is naturally combined with the frozen-core approximation separating valence and core spaces. However, one may argue that it introduces at the same time an additional error from neglecting core correlation.[31,103]

2.3. Implementation Details. In this work, we focus on exploring the definition of different CVS variants and assessing their performance following the projection-based scheme, due to its ease of implementation, and with it in view of later implementing the analytical CVS[31] formulation in DIRAC.

We have based our implementation on a flexible scheme to define projection operators.

(a) A mapping is defined between the excited determinants (and the virtual and occupied spinors' energies associated with each) and the position of each excited determinant in the storage of the ground-state CC amplitudes and EOM-CC coefficients (in the RELCC module of DIRAC, these are stored in triangular forms, and blocked by symmetry, for details see refs 106−108).

(b) Information is gathered on how the excited determinant space $\{\nu\}$ will be treated, i.e., whether retained ($P^\nu = 1$) or projected out ($P^\nu = 0$). We have made two options available to the user, based on spinor energies ϵ: (i) restricted excitation windows (REWs) for the occupied and virtual, which are defined by setting respective lower (ϵ_L) and upper (ϵ_H) bounds for the spinor's energies and (ii) CVS, via a single energy that acts as the threshold (ϵ_{CV}) for the separation between core and valence.

(c) Using the information from the previous steps, suitable one-particle (singly ionized or excited) unit trial vectors for the core states are then generated, using the values of the diagonal of $\bar{H}$ within the subspaces defined in (b).

It is important to note that in our implementation, tracking the core-excited or -ionized states requires the use of a root homing procedure, in which new trial vectors are created by maximizing their overlap with the preceding ones.

In addition to CVS and REW for the excited states, we also used the projection setup to implement the frozen-core approximation, such that we can project out the amplitudes corresponding to core (c) orbitals at each iteration during the resolution of the ground-state amplitude equations

$$P^{\text{core}}|\Psi_{CC}\rangle \Rightarrow t_i^a = t_{ij}^{ab} = 0 \text{ if } i, j \in c \tag{17}$$

As for the excited states, this projector is defined in terms of spinor energies, via a single threshold or upper and lower bounds defining a window. Finally, it should be noted that the thresholds defining the ground-state and excited-state projectors are independent.

3. COMPUTATIONAL DETAILS

All coupled-cluster calculations were carried out with the DIRAC electronic structure code[85] (with the DIRAC19[109] release and revisions `dbbfa6a`, `0757608`, `323ab67`, `2628039`, `1e798e5`, `b9f45bd`). The Dyall basis sets[110−112] of triple-zeta quality (dyall.acv3z) were employed for all species. For selected calculations, on heavy atoms only, we performed extrapolations to the complete basis set limit by also considering quadruple-zeta quality Dyall (dyall.acv4z) basis sets. In addition to the Dyall basis sets, the ANO-RCC basis[113] were employed for Xe and XeF_2. The basis sets were kept uncontracted in all calculations.

Unless otherwise noted, all occupied and virtual spinors were considered in the correlation treatment.

Apart from the Dirac−Coulomb (^{4}DC) Hamiltonian, for selected calculations, we investigated: (a) the molecular mean-field[79] approximation to DC (^{2}DC^M) and the Dirac−Coulomb−Gaunt (^{2}DCG^M) Hamiltonians. For the latter, the Gaunt-type integrals are explicitly taken into account only during the four-component SCF step due to the fact that the transformation of these to MO basis is currently not implemented; (b) the DC Hamiltonian with projecting out all negative-energy solutions of the bare-nucleus one-electron Dirac Hamiltonian from the molecular spinor space, which corresponds to the Furry basis for quantum electrodynamics (QED) and no-pair Hamiltonians[114] (^{4}DC^{PF}); and (c) the exact two-component (X2C)[76] Hamiltonian, in which we include two-electron spin−orbit contributions to the untransformed two-electron potential via atomic mean-field contributions calculated with the AMFI code,[115−117] namely, spin-same-orbit (X2C-AMFI) and spin-same-orbit and spin-other-orbit (X2C-G-AMFI).

Unless otherwise noted, we employed the usual approximation of the energy contribution from (SS|SS)-type two-electron integrals by a point-charge model.[118] As will be discussed below, this approximation introduces negligible errors (<0.01 eV) for lower-energy edges. However, for the higher-energy edges of the heavier systems, its error becomes important.

The XeF_2 structure was taken from ref 119. It corresponds to an optimized structure obtained at the SFX2C-1e/coupled-cluster single double triple (CCSD(T))/unc-atomic natural orbital (ANO)-RCC level ($r_{Xe\text{-}F}$ = 1.9736 Å). The coordinates of CH_3I come from the experimental data in ref 120. Finally, the coordinates for HX were taken from ref 121.

The dataset can be retrieved at the Zenodo repository.[122]

3.1. Approximations Used in CVS. Besides the original CC-CVS approach,[28] we have also investigated other approximations:

1. Further restricting the definition of the projectors to also drop excited configurations with two core indices (ND, for "No Doubly core hole determinants"); this corresponds to the method suggested, e.g., in ref 40, obtaining

$$^\mu r_{ij}^{ab} = 0 \text{ if } i, j \in c \tag{18}$$

2. Freezing the core in the ground-state calculation, thus retaining only the valence orbitals, typically defined as the orbitals with the highest principal quantum number n (FC-V); this essentially corresponds to using eq 17 while setting ϵ_{CV} to a fairly high value (for example, in the atom of Xe, $\epsilon_{4d} < \epsilon_{CV} < \epsilon_{5s}$).

3. Freezing all core orbitals, except for those that are to be targeted in the EOM step (FC-V-except); for example, this means treating a core spinor k, that should make up the most important core-excited configurations for state μ, different from other core spinors in the ground-state calculation. This corresponds to setting projectors for ground and excited states such that

https://doi.org/10.1021/acs.jctc.0c01203
J. Chem. Theory Comput. 2021, 17, 3583−3598

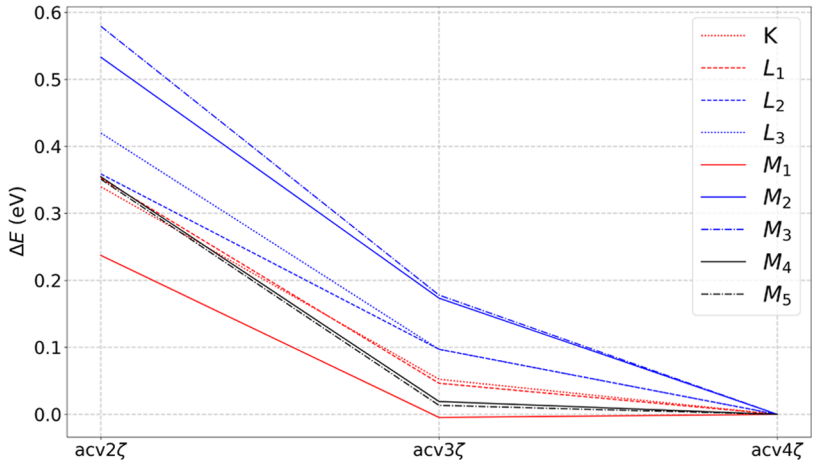

Figure 1. Basis set influence (Dyall basis sets) on the core binding energies of I^- using the CVS approach. All calculations performed with the $^2DC^M$ Hamiltonian, and basis sets are kept uncontracted.

$$t_i^a = t_{ij}^{ab} = 0 \text{ if } \begin{cases} i, j \neq k \\ i, j \in c \end{cases} \tag{19}$$

$$^{\mu}r_i^a = {}^{\mu}r_{ij}^{ab} = 0 \text{ if } i, j \in v \tag{20}$$

This approach is equivalent to the one of Sorensen et al.[103]

4. The definition of the core/valence spaces follows that of the CVS definition/threshold, that is, only the core orbitals with the same or lower energy than the ones belonging to the edge under investigation are frozen (FC-f). This is the same approach adopted in ref 31, and it corresponds to setting projectors for ground and excited states such that

$$\text{if } i, j \in v \begin{cases} t_i^a = t_{ij}^{ab} & = 0 \\ {}^{\mu}r_i^a = {}^{\mu}r_{ij}^{ab} & = 0 \end{cases} \tag{21}$$

5. Further restricting the number of frozen-core spinors to only those below the ones of the edge of interest (FC-fpMO frozen core—follow previous MO). For example, in the atom of Xe, if we are interested in the M_5 edge ($3d_{5/2}$), this would correspond to a frozen core in the ground-state calculation, including the $1s_{1/2}$ to $3d_{3/2}$ spinors, and the $4s_{1/2}$ and higher spinors make up the valence space in the EOM calculations.

The variants ND and FC-V were also employed with REWs. Since the performance of REW variants was always found to be inferior to their CVS equivalents, they will not be discussed here. The results are, however, available as the Supporting Information.

4. RESULTS

As outlined above, apart from the different Hamiltonians at our disposal, the original CVS formulation itself can be modified through a number of different approximations. To draw a clearer picture of their interactions, we proceed in a stepwise manner: first, using the $^2DC^M$ Hamiltonian and focusing on core ionizations, we compare (A) the performance of CVS-EOM-CCSD to the original EOM-CCSD; and (B) the impact of the different approximations that can be introduced in the CVS method itself (see Section 3.1). Then, having established the relative accuracy of CVS, we investigate (C) the effect of the Hamiltonians on the core-ionization energies, and finally (D) proceed to a comparison to experiment of the most accurate setup, focusing mostly on core ionizations and also discussing selected core excitations (E).

In what follows, we will not discuss basis set effects. Nonetheless, in Figure 1, we show for I^- a typical behavior: first, there is very little difference between triple- and quadruple-zeta results (with differences between 0.05 and 0.2 eV), making the corrections, due to basis set incompleteness, so small that we consider these to be unnecessary. Second, if there are non-negligible differences between the convergence of s, p, and d shells as the basis sets are improved, the double-zeta basis sets also yield results that are quite good, with differences in binding energies with respect to the triple-zeta results no larger than around 0.4 eV, a behavior that may make these smaller basis sets interesting for calculations on larger molecules.

These conclusions are in line with earlier basis set analyses on light elements.[64,123] In the basis set convergence study by Sarangi et al.,[123] in particular, it was shown that, for systems containing only light elements, uncontracted basis sets, even of relatively modest quality for the valence, can provide quite reliable core binding energies.

4.1. Comparison of CVS-EOM-IP-CCSD and EOM-IP-CCSD. As mentioned above, the CVS approach provides an efficient and robust way of targeting the low-lying core states. Quantifying the errors introduced by it is therefore an important issue, and we note proposals for methods to estimate it. Coriani and Koch[28] evaluated the errors of their CVS variant by comparing to full-space Lanczos results, finding deviations of at most a few hundredths of eV. The authors also proposed a perturbative correction obtained using a Löwdin partition of the Jacobian and the eigenvalue equation. A recent study by Herbst and Fransson[124] shows that the CVS error is small and stable across multiple systems within the algebraic diagrammatic method (ADC). Thus, we expect to find the same trend for CC. This article also reports the implementation of a postprocessing step, which removes the error to assess its significance.

Here, we can harness the ability of DIRAC to exploit linear symmetry, and directly compare, for selected species, the CVS-EOM-IP-CCSD states with those obtained by the full diagonalization of the different symmetry blocks of the similarity-transformed Hamiltonian.

https://doi.org/10.1021/acs.jctc.0c01203
J. Chem. Theory Comput. 2021, 17, 3583−3598

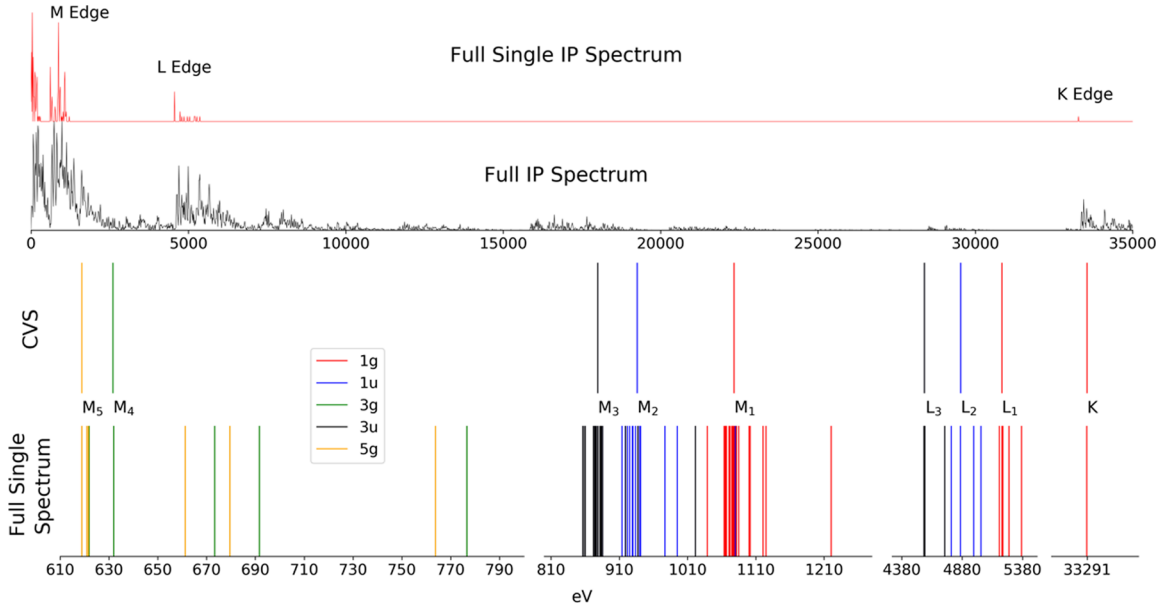

Figure 2. Core-ionization energies of iodide (I^-) from full diagonalization of $\bar{H}$. (Top) Representation of the eigenspectrum up to 35 keV, separated between all states (black) and those with non-negligible singly ionized contributions (red). Values in ordinate correspond to the number of states within a 10 eV interval, with the largest value rescaled to one. (Bottom) Singly ionized states obtained by full diagonalization of $\bar{H}$ and by the core−valence separation (CVS) approach. The labels ng/nu indicate the absolute value for the projection of the angular momentum ($|m_j| = n/2$, $n = 1, 3, 5$) and for the components of spinors of gerade (g) or ungerade (u) symmetry. All calculations are performed with the $^2DC^M$ Hamiltonian.

The difference between the two approaches is shown graphically for I^- in Figure 2. Due to the very dense spectra of $\bar{H}$, in the top half of the figure, we do not display individual states but rather the number of states per 10 eV intervals. We further discriminate between all states (black) and those containing contributions from singly ionized configurations contributing to at least 1% of the total wave function (red).

Upon having a closer look at the singly ionized states at the bottom half of the figure, we can more clearly see how the singly ionized states obtained with the CVS approximation (labeled "CVS") closely match a subset of those obtained by the full diagonalization (labeled "full") of $\bar{H}$.

We note that the additional states presented for the full calculation correspond not only to states that contain significant singly ionized characters but also small but nonzero $2h1p$ contributions. The presence of such states hints at potential pitfalls when targeting only a subset of such highly excited states for some of the L and M edges—not so much in terms of convergence (we have not encountered particular difficulties in converging our calculations) but rather in terms of assignment and comparison to other theoretical or experimental results.

4.2. Performance of the CVS-EOM-CCSD Variants. Next, we turn our attention to the performance of the different approximations that can be employed on top of CVS (see Section 3.1 for their description). Our results for the X^- systems are shown in Figure 3. As we see similar trends for Xe, the corresponding figure is shown in the Supporting Information (Figure S1), along with results for the REW approach for the Cl^- to I^- (Figures S2−S4) and HCl to HI (Figures S5−S7).

4.2.1. Freezing Core Orbitals in the Ground State. Freezing the core orbitals in the ground-state CCSD calculation results in a significant lowering of the core-ionization energies. This lowering is considerable if the frozen core is taken to represent all subvalence spinors (FC-V), and it remains non-negligible even if the same threshold is used to define both the frozen orbitals and the core−valence separation region (FC-f). However, if one does not freeze the aimed edge (FC-fpMO), the ionization energy obtained is much closer to the corresponding CVS one.

Freezing all subvalence spinors but the ones in the edge we are interested in (FC-V-ex), an approximation that could provide potentially lower computational cost for systems with a large number of core electrons, such as the elements in the fourth row and beyond, does not perform better than (FC-f)—in fact, the opposite appears to be the case for the inner core orbitals.

4.2.2. Projecting Out Double-Core-Ionized Configurations. Projecting out doubly excited core-excited determinants (ND) tends to result in an increase of the core-ionization energies, which can be significant though always smaller than the underestimation produced by freezing all of the core spinors.

As a result, the combination of these two approximations leads to an approximate scheme that much better reproduces the CVS energies, though still with non-negligible discrepancies for the heavier elements. Particularly good results are shown by the (FC-ND-f) combination, for which error compensation yields results very similar to the regular CVS approximation. This can be rationalized because core correlation is not taken into account when using (FC-f), whereas the inclusion of the double occupied core orbitals in the EOM step does. Therefore, the combination of both approximations is in fact more consistent.

4.2.3. Efficiency Considerations. Since by using projection operators we do not save in memory or operation counts, the approximations discussed above are not of strong interest by themselves, and will not be used further since, even in the best combination, they will invariably degrade the performance of the original CVS scheme.

We can nevertheless use our findings to discuss the potential trade-offs between cost and accuracy, as a guide to efficient implementations such as those proposed in ref 31 for heavy elements. As discussed then, combining the elimination of doubly core-excited determinants with the use of a frozen core (FC-ND-f, which is equivalent to the scheme in ref 31) seems to

https://doi.org/10.1021/acs.jctc.0c01203
J. Chem. Theory Comput. 2021, 17, 3583−3598

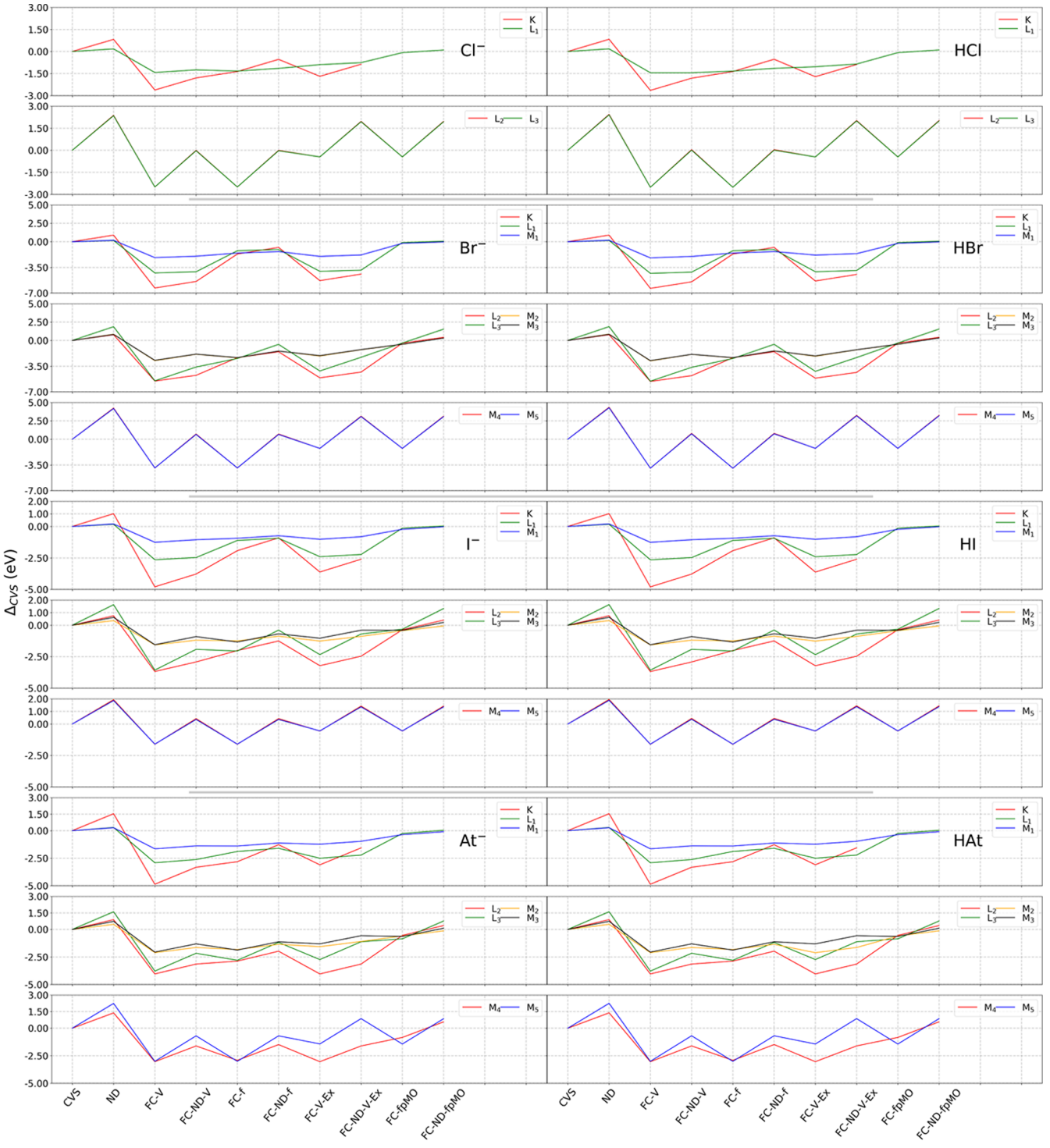

Figure 3. Effect of the CVS variants on the binding energies of X^- and HX systems (X = Cl, Br, I, and At). Values (in eV) are relative to the original CVS approach. All calculations are performed with the $^2DC^M$ Hamiltonian.

result in a computationally efficient approach with a good error cancellation balance, and this remains the case as one goes down the periodic table.

In the case of heavy elements, it may also be interesting to keep a large frozen core (CVS-FC-ND-V or CVS-FC-V-Ex) since these introduce non-negligible but seemingly systematic errors with the advantage that a large core would translate in potentially large computational savings.

This is illustrated in Table S1, where we provide, for the representative systems Cl^- and At^-, the operation counts (without reductions due to point group symmetry) for the construction of EOM-EE and EOM-IP σ vectors (based on the expressions from Shee et al.,[84] see expressions in the Supporting Information), in the case of an analytical implementation of the major approximations suggested in this work (FC-f and ND). As seen, the FC-f approximation results in the biggest reductions in operation counts, in particular for EOM-IP. It is also important

https://doi.org/10.1021/acs.jctc.0c01203
J. Chem. Theory Comput. 2021, 17, 3583−3598

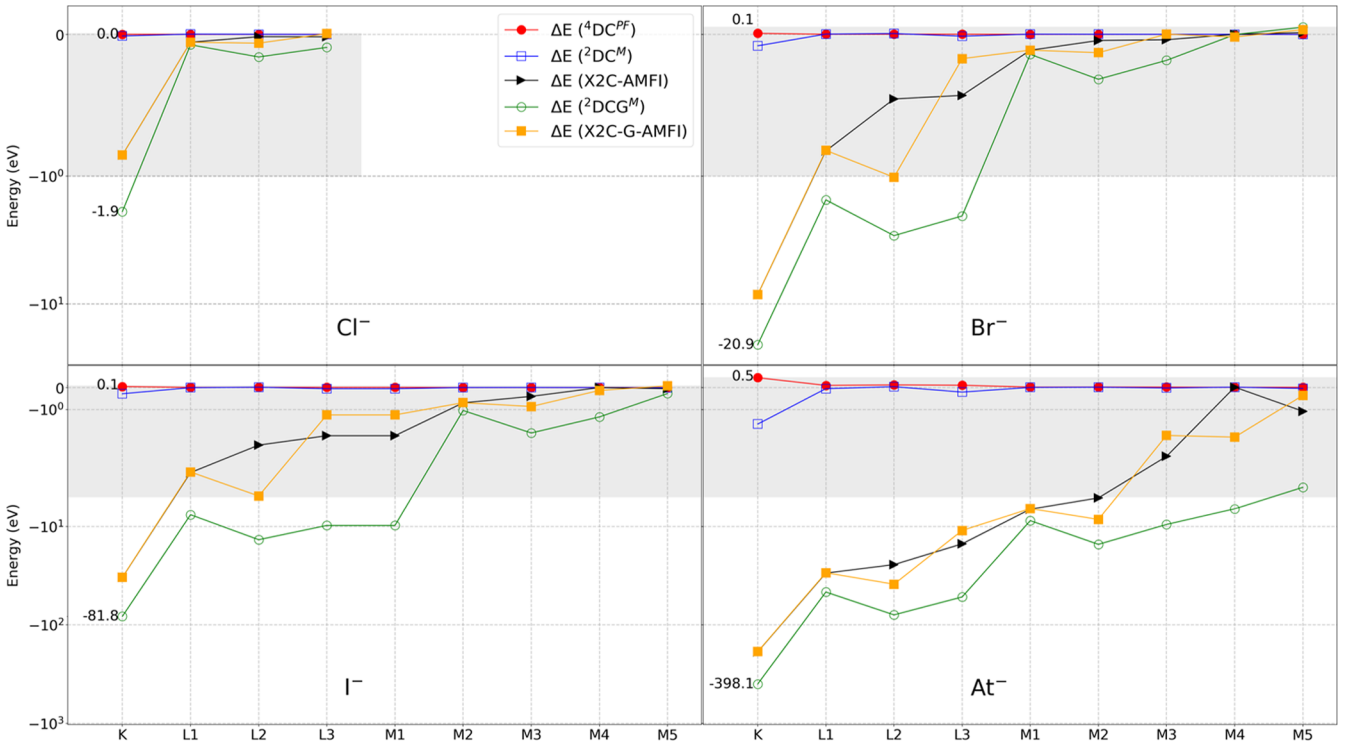

Figure 4. Comparison of the influence of the Hamiltonian to the core binding energies for different edges, for the halide ions (Cl^- to At^-). Instead of binding energies themselves, we present the difference between the binding energies obtained for each Hamiltonian X and ^{4}DC ($\Delta E_m(X) = E_m(X) - E_m(^4\text{DC})$, in eV, m a particular edge). The scales are logarithmic, except for the areas in gray for which the scales are linear.

Table 1. MP2 and CCSD Correlation Energies as well as Differences in Correlation Energy between ^{4}DC (E_c and ΔE_c, Respectively, in eV), for Different Hamiltonians[a]

		^{4}DC^{PF}	^{2}DC^M	^{2}DCG^M	X2C(a)	X2C(b)
Cl^-	E_c(MP2)	−16.12	−16.16	−16.16	−16.16	−16.16
	ΔE_c	$<2 \times 10^{-6}$	−0.04	−0.04	−0.04	−0.04
	E_c(CCSD)	−16.43	−16.47	−16.47	−16.47	−16.47
	ΔE_c	$<2 \times 10^{-6}$	−0.04	−0.04	−0.04	−0.04
Br^-	E_c(MP2)	−41.44	−41.65	−41.64	−41.65	−41.65
	ΔE_c	$<5 \times 10^{-5}$	−0.21	−0.20	−0.21	−0.21
	E_c(CCSD)	−39.65	−39.86	−39.85	−39.86	−39.86
	ΔE_c	$<5 \times 10^{-5}$	−0.21	−0.20	−0.21	−0.21
I^-	E_c(MP2)	−48.54	−49.07	−49.05	−49.06	−49.06
	ΔE_c	$<3\times 10^{-4}$	−0.53	−0.51	−0.52	−0.52
	E_c(CCSD)	−46.13	−46.65	−46.64	−46.65	−46.65
	ΔE_c	$<3 \times 10^{-4}$	−0.52	−0.51	−0.52	−0.52
At^-	E_c(MP2)	−90.95	−92.90	−92.83	−92.86	−92.87
	ΔE_c	$<3 \times 10^{-3}$	−1.95	−1.88	−1.91	−1.92
	E_c(CCSD)	−84.30	−86.24	−86.17	−86.20	−86.20
	ΔE_c	$<3 \times 10^{-3}$	−1.94	−1.87	−1.90	−1.91

[a]X2C(a) refers to X2C-AMFI and X2C(b) to X2C-G-AMFI.

to note that for a given edge, the heavier the element, the bigger these reductions are.

4.3. Influence of the Hamiltonian on the Core Ionizations. We now turn our attention to the impact of the Hamiltonian on ionization energies. Our results can be found in Figure 4, where we take the ^{4}DC Hamiltonian as a reference and plot the difference in binding energies between it and the other Hamiltonians considered (see the figure caption for details), as ^{4}DC is the only four-component Hamiltonian without approximations (apart from the treatment of the (SS|SS) integrals, which we address below), we can employ in correlated calculations with DIRAC.

First, we observe a very good match between the ^{4}DC and ^{2}DC^M Hamiltonians across the halogen series—that is, differences in absolute values generally fall below 0.001 eV for the M edges, between around 0.01 and 0.1 eV for the L edges, and are of the order of 0.1 eV for the K edge of all species, except for astatine, for which the difference is 1.67 eV. This latter discrepancy is still small compared to the K edge binding energy of 96 keV.

https://doi.org/10.1021/acs.jctc.0c01203
J. Chem. Theory Comput. 2021, 17, 3583−3598

To better understand how these discrepancies arise, we should recall that in the $^2DC^M$ ($^2DCG^M$) approximation, a calculation with the ^4DC (^4DCG) Hamiltonian is first carried out for whatever system we are interested in, in general, a molecule, hence, the denomination "molecular mean-field", though in Figure 4, we are in effect dealing with atoms. Upon convergence, the transformation into two-component is carried out on the Fock matrix itself (so that the two-component spinor energies correspond exactly to the four-component ones) but the two-electron operator is left untransformed[79,85] and thus introduces a picture-change error in the electron−electron interaction. In valence only calculations, where core−core and core−valence electron correlation is not accounted for, this yields negligible errors for excitation, ionization, and electron attachment processes.[84] Our results show that this is still the case for core states of light atoms, such as chloride, and for the M and N edges down to the sixth row.

We can numerically assess the effect of using an untransformed two-electron operator by comparing how the correlation energy (E_c) differs between $^2DC^M$ and ^4DC (ΔE_c), as shown in Table 1. The ΔE_c for both MP2 and CCSD yields the same trends; therefore, we shall focus on the simpler MP2 model; as canonical orbitals are employed and their energies are the same for $^2DC^M$ and ^4DC, any differences between the two come from the picture-change error in the two-electron integrals. We see that for chloride, ΔE_c is still relatively small, then it increases 5-fold going from chloride to bromide, doubles from bromide to iodide, and then increases nearly fourfold from iodide to astatide.

The effect of the two-electron picture-change error can also be seen through a comparison of ^4DC to a calculation in which negative-energy solutions of the bare-nucleus one-electron Dirac Hamiltonian are projected out from the molecular spinor space ($^4DC^{PF}$), whereby rotations between the negative and positive energy states are effectively eliminated. With this, $^4DC^{PF}$ spinor energies are slightly different from the ^4DC ones (see dataset[122]), but the picture-change error in the two-electron integrals is eliminated, and we would thus expect rather similar correlation energies. This picture is consistent with our numerical results, as correlation energies for $^4DC^{PF}$ are closer to the ^4DC ones by at least three orders of magnitude than the $^2DC^M$ ones.

As it will be shown in the following, the sufficiently high accuracy of $^2DC^M$ clearly makes it an asset for applications, due to its reduced computational cost in the index transformation step. However, our results indicate that two-electron picture-change errors are significant enough for deeper cores to require further attention for elements in the sixth row and beyond.

While we do not have ^4DCG reference values to which we compare the approximate Hamiltonians that include the Gaunt interaction such as $^2DCG^M$, we expect two-electron picture-change errors to generally follow the same trends discussed above. We, nevertheless, compare $^2DCG^M$ to ^4DC in Figure 4 and Table 1, as a way to underscore the importance of the Gaunt interaction for the inner edges. We clearly see that already starting with chloride, we have a non-negligible effect arising from the Gaunt interaction in $^2DCG^M$ that lowers the core binding energy, and can amount to nearly 2 eV for the K edge with respect to the $^2DC^M$ or ^4DC.

We can also compare $^2DCG^M$ to the approaches in which the transformation to the two-component picture is done before the SCF step (X2C-AMFI and X2C-G-AMFI), as opposed to using the full atomic or molecular potential obtained from the SCF step as in the $^2DCG^M$ approach. We see that the latter qualitatively follow the changes in binding energy seen for $^2DCG^M$ as we move across the rows, though with significant numerical differences for the K edge (with differences of over 40 eV for iodine and xenon, and over 200 eV for Astatine) as well as for the L and M edges.

Finally, we assess the effect of including the (SS|SS) integrals in $^2DC^M$ and $^2DCG^M$ calculations. Since these contributions are generally very small for elements before the fourth row, and they significantly increase the cost of the SCF step, we have only investigated the fourth- and fifth-row atoms (I, Xe, and At) (Table 2).

Table 2. Contributions (in eV) to the Core Binding Energies of I^-, Xe, and At^- from (a) the Gaunt Interaction and (b) the (SS|SS) Integral[a]

	I^-		Xe		At^-	
edge	ΔE(a)	ΔE(b)	ΔE(a)	ΔE(b)	ΔE(a)	ΔE(b)
K	−81.57	−2.58	−86.75	−2.87	−396.04	−40.50
L_1	−7.59	−0.39	−8.15	−0.44	−46.24	−7.28
L_2	−13.64	−0.58	−14.62	−0.65	−78.99	−10.46
L_3	−9.70	−0.21	−10.39	−0.23	−51.77	−3.56
M_1	−1.05	−0.08	−1.14	−0.09	−8.72	−1.79
M_2	−2.08	−0.21	−2.25	−0.12	−15.19	−2.35
M_3	−1.34	−0.08	−1.46	−0.04	−9.51	−0.89
M_4	−0.59	−0.06	−0.66	−0.03	−6.62	−0.82
M_5	−0.26	−0.04	−0.31	0.01	−4.52	−0.09
N_1					−1.81	−0.44
N_2					−3.29	−0.55
N_3					−1.81	−0.19
N_4					−0.91	−0.10
N_5					−0.42	0.02
N_6					6.74	0.06
N_7					0.48	0.12

[a]These contributions are calculated as the energy difference between CVS-EOM-CCSD calculations employing (a) the $^2DCG^M$ and $^2DC^M$ Hamiltonians and (b) the $^2DCG^M$ without and with the inclusion of the (SS|SS) integrals at the SCF step.

For I^- and Xe, these contributions are relatively modest, with reductions of around 2.6 eV and 3 eV to their K edge binding energies, with other significant reductions for the L (0.4−0.7 eV) and $M_{1,2}$ edges (0.1 eV). We note that there is little variation from these atomic values for the molecular systems (see dataset[122]), in line with the much more localized nature of the small-component density compared to the large component one. Furthermore, we notice a very subtle difference (0.02 eV) between the $^2DC^M$ and $^2DCG^M$ Hamiltonians with (SS|SS) integrals.

For At^-, the reductions in binding energies are much more significant: around 40 eV for the K edge, 10 eV for the L_2 edge, and well above 1 eV for the L_3 to M_2 edges. Interestingly, these contributions remain around 0.5 eV for the N edges relating to ionizations from s and p spinors, which are comparable to the energies of the M_1 and M_2 edges for I^- and Xe, which fall between 0.7 and 1 keV.

These results underline the need for explicitly accounting for these integrals (or correcting the energies for their contribution), as soon as we are interested in edges arising from ionizations of s and p spinors for fifth-row elements and beyond.

4.4. Binding Energies: Comparison to Experiment and Prior Theoretical Works. We now compare our results for the

https://doi.org/10.1021/acs.jctc.0c01203
J. Chem. Theory Comput. 2021, 17, 3583−3598

$^2DC^M$ and $^2DCG^M$ Hamiltonians, including the (SS|SS) integrals, to experiment and other theoretical results for the K and L edges of Xe, XeF_2, and CH_3I, for which recent high energy, gas-phase XPS experiments have been performed (for Xe and XeF_2, results are also available for less energetic edges). Our results are found in Table 3.

Table 3. Comparison between Calculated and Experimental Gas-Phase Binding Energies (in eV) for Xe, XeF_2, and CH_3I[a]

edge	model	E(a)	E(b)	E(c)	E(d)
		Xe			
K	D/^{4}DC	34 755.91	34 690.82	34 567.44	34 563.64
	D/^{2}DC^M	34 755.91	34 690.60	34 567.22	34 563.42
	D/^{2}DCG^M	34 669.08	34 603.85	34 567.22	34 563.42
	A/^{4}DC	34 755.89	34 690.63	34 567.48	34 563.68
	A/^{2}DC^M	34 755.89	34 690.63	34 567.24	34 563.44
	A/ref 127	34 752.00	34 690.90	34 567.51	34 563.71
	exp.[127]				34 565.13
L_1	D/^{2}DC^M	5509.35	5473.66	5460.49	
	D/^{2}DCG^M	5501.17	5465.51	5460.49	
	exp.[128]				5452.7
L_2	D/^{2}DC^M	5161.45	5122.38	5109.30	
	D/^{2}DCG^M	5146.77	5107.77	5109.30	
	exp.[128]				5106.7
L_3	D/^{2}DC^M	4835.59	4796.85	4787.51	
	D/^{2}DCG^M	4825.15	4786.46	4784.51	
	exp.[128]				4786.7
M_4	D/^{2}DC^M	708.13	689.63	689.01	688.31
	D/^{2}DCG^M	707.46	688.98	689.01	688.31
	A/ref 127	707.5	689.6	688.98	688.28
	exp.[127]				689.23
M_5	D/^{2}DC^M	694.90	676.71	676.32	675.62
	D/^{2}DCG^M	694.58	676.30	676.32	675.62
	A/ref 127	694.6	676.7	676.08	675.38
	exp.[127]				676.44
		XeF_2			
K	D/^{4}DC	34 759.79	34 694.48	34 567.08	34 566.18
	D/^{2}DC^M	34 759.79	34 693.30	34 569.90	34 566.00
	A/^{2}DC^M	34 759.76	34 694.28	34 570.89	34 566.99
	A/ref 127	34 755.80	34 694.50	34 571.10	34 567.20
	exp.[127]				34 567.4
M_4	D/^{2}DC^M	711.99	693.23	692.61	691.61
	A/^{2}DC^M	711.74	693.32	692.70	691.70
	A/ref 127	711.9	693.9	693.28	692.28
	exp.[129]				692.09
M_5	D/^{2}DC^M	698.49	680.22	679.93	678.93
	A/^{2}DC^M	698.46	680.30	680.01	679.01
	A/ref 127	698.6	680.6	680.31	679.31
	exp.[129]				679.31
		CH_3I			
K	D/^{2}DCG^M	33 278.46	33 213.79	33 180.89	
	exp.[130]				33 175.20
L_1	D/^{2}DCG^M	5244.04	5208.55	5203.95	
	exp.[130]				5197.47

[a]Calculations are broken down into values obtained with (a) Koopmans theorem, (b) CVS-EOM-CCSD method; (c) CVS-EOM-CCSD with atomic corrections for QED and Breit (in the case of $^2DCG^M$ results, corrections for the gauge term) interactions; and (d) higher-order correlation corrections by Southworth and co-workers on (c). All of our results include contributions from the (SS|SS) integrals. Basis sets A: ANO-RCC and D: Dyall.

As all our calculations lack contributions from QED effects, and $^2DCG^M$ does not include the gauge term that is necessary to recover the full (zero-frequency) Breit interaction, we correct our energies with the results from Kozioł and Aucar,[125] who provided the values for the Breit and leading QED contributions (self-interaction and vacuum polarization) to the atomic spinors of the selected closed-shell atoms (among which is Xe). The same procedure was followed by Southworth et al.[126] to correct their calculations, which are based on a combination of one-component CVS-EOM-CCSD (and CCSDT) calculations with energy estimates for different effects (1- and 2-electron scalar relativity, spin−orbit coupling, nuclear size effects).

Taking the Xe atom, the QED effects are most important for the K and L_1 edges, lowering the associated binding energies by 42.7 and 5.5 eV, respectively. They are also non-negligible for the L_3 and M_1 edges, which are lowered, respectively, by 0.5 and 1.1 eV. The Breit interaction also lowers the binding energies and, apart from the L_1 edge (for which both are of the same magnitude), is in general much larger than the QED effects (80.7, 13.1, and 8.8 eV for the K, L_2, and L_3 edges, respectively) and still important for the M_3 edge (1.2 eV).

Since Kozioł and Aucar only provide the full Breit term, we have estimated the magnitude of the gauge correction from the difference between our $^2DCG^M$ results and their Breit values. From that, we have that the gauge term increases the binding energies (6.04 eV for the K edge, 0.51 eV for the L_1 edge, and around 1.57 and 1.58 eV for the L_2 and L_3 edges, respectively).

We observe that our corrected two-component results differ from the experiment by around 2.1 eV, and if we employ the estimate for higher-order correlation contributions to EOM-CCSD from Southworth et al.,[126] which decreases the binding energies by 3.8 eV, the difference to experiment is now of −1.71 eV.

We have also investigated the use of uncontracted ANO-RCC basis, used by Southworth et al.,[127] which is slightly smaller for s and p primitive sets than the Dyall sets. We obtain differences with respect to the experiment of −1.69 eV, which is consistent with our results using the Dyall basis sets. We attribute most of the small differences between ours and prior results to the shortcomings in the treatment of the two-electron interactions in $^2DC^M$ or $^2DCG^M$ discussed previously, as calculations with ^{4}DC yield results in very good agreement with those of Southworth et al.

Beyond the K edge, our corrected calculations compare rather well to the recent experimental results of Oura et al.[128] (5452.7, 5106.7, and 4786.7 eV; measurements carried out at BL29XU of SPring-8 in May 2016) with the exception of the L_1 edge, for which a larger discrepancy to experiment (7.79 eV) is observed. For the M edges, Southworth et al.[127] present experimental results for the $M_{4,5}$ edges, and our corrected calculations differ from the experiment by −0.94 and −0.85 eV respectively. For the M_4 edge, these are quite comparable to the theoretical calculations of Southworth and co-workers,[127] now also corrected for QED effects (−0.92 eV to experiment), while for the M_5 edge both theoretical results differ by around 0.24 eV.

Given the values for the higher-order correlation effects for the K and $M_{4,5}$ edges, and from the breakdown of relativistic, correlation, and QED effects from atomic many-body calculations on Xe at the K, L, and M edges[131]—which indicate non-negligible differential correlation, relaxation, and other effects (for example Auger shifts) for the different L edges, and to a lesser extent for the M edges—we consider future attempts

https://doi.org/10.1021/acs.jctc.0c01203
J. Chem. Theory Comput. 2021, 17, 3583−3598

to investigate higher-order electron correlation corrections for the L edges to be of significant interest.

For XeF_2, applying the same corrections as above to our $^2DC^M$ and $^2DCG^M$ calculations in the Dyall basis sets, we arrive at K and $M_{4,5}$ edge binding energies differing by roughly −0.4 eV from the experiment. These differences are smaller but consistent with those obtained for Xe, underscoring the largely atomic nature of these deep core energies. As was the case for the atom, a comparison to ^{4}DC results for the K edge indicates that part of the small differences between the results of Southworth et al. and our two-component ones come from the shortcomings in the treatment of two-electron interactions.

For CH_3I, we have only performed $^2DCG^M$ calculations first because, as illustrated above, there are no significant differences between $^2DCG^M$- and $^2DC^M$-based results once we account for QED and Breit or gauge contributions. Second, in the C_s point group used, the coupled-cluster wave functions are complex-valued, making calculations computationally more expensive. We obtained 33213.79 and 5208.55 eV for the K and L_1 edge binding energies, values that overestimate the experimental values by 38.59 and 11.08 eV. For the K edge, this difference is rather close to the one found for the Xe and XeF_2 species.

As QED and Breit corrections are not provided by Kozioł and Aucar[125] for iodine, we have instead used those of Boudjemia et al.,[130] which amount, for the K edge, to −77.0 eV for Breit, +6.10 eV for the gauge term, and −39.0 eV for QED, and to −7.20, +0.50, and −5.10 eV for the L_1 edge. With these corrections, we now overestimate the K and L_1 binding energies by 5.69 and 1.95 eV. The missing effect would be that of higher-order correlation corrections. However, we cannot estimate this here, and we speculate that if it follows roughly what is found for the Xe species, it would decrease the binding energies and likely take the K edge to a few eV.

4.5. Excitation Energies: Comparisons to Experiment and Prior Theoretical Works. As anticipated, the current implementation allows calculation not only of ionization energies but also of excitation energies, which will be briefly discussed hereafter. In this case, since (SS|SS) integrals do not significantly affect the energies, only results for the $^2DCG^M$ and $^2DC^M$ Hamiltonian are presented, without explicit inclusion of the aforementioned integrals.

The results are shown in Table 4, which displays selected excitation energies from different edges to the lowest unoccupied molecular orbital (LUMO). We chose these particular transitions since both experimental and computational data are available in the literature,[126,127] which can be used as reference values. In particular, the experimental values are tabulated with the theoretical energies obtained in this study.

As already observed for the ionization processes, the inclusion of the Gaunt interaction, accounting for the magnetic interaction between the electrons, lowers the excitation energy. This was expected as, in general, the inclusion of this term shifts the orbital energies of the inner core orbitals up (or lowers them, in term of absolute energy) and, at the same time, it reduces the spin−orbit coupling,[62] which is also reflected by the results reported herein. Indeed, the difference in the excitation energy from $3d_{3/2}$ and $3d_{5/2}$ to LUMO is slightly higher when the $^2DC^M$ Hamiltonian is employed.

Upon inclusion of the Gaunt term in the Hamiltonian, the excitation energies differ by at most 0.4% from the corresponding experimental value, specifically for 1s(F). This mismatch is higher than the others, which can be due to the fact that the CVS space was reduced so that this was the highest orbital, necessary to get this excitation.

Thus, this space excludes the 3d orbitals and in particular $3d_{3/2}$. The next higher disagreement between theory and experiment is found when exciting the 1s(Xe), although by only 0.1%. Finally, the best agreement is found for both 3*d* orbitals, with an error of only 0.04% ($3d_{3/2}$) and 0.02% ($3d_{5/2}$) from experiment. The computed energies are thus within the experimental error. To obtain the excitation from the ($3d_{3/2}$) orbital, the same strategy of excluding all higher orbitals from the CVS space, hence excluding ($3d_{5/2}$), might be the reason for the subtly larger disagreement.

Nonetheless, these errors are actually quite small. Therefore, we can conclude that the CVS-EOM-CC method implemented in this work gives satisfactory core-excitation energies.

Table 4. XeF_2[a]

edge	transition	model	*E*
K	1s (Xe) → LUMO	D/$^2DC^M$	34 686.70
	D/$^2DCG^M$		34 599.95
	exp.[126]		34 557.4
	1s (F) → LUMO	D/$^2DC^M$	685.91
	D/$^2DCG^M$		685.70
	exp.[127]		682.8 ± 0.3
M_4	$3d_{3/2}$ → LUMO	D/$^2DC^M$	683.71
	D/$^2DCG^M$		683.06
	exp.[127]		682.8 ± 0.3
M_5	$3d_{5/2}$ → LUMO	D/$^2DC^M$	670.34
	D/$^2DCG^M$		670.04
	exp.[127]		669.9 ± 0.3

[a]Comparison between the experimental gas-phase excitation energies and calculations (in eV). The calculated excitation energies have been obtained at the CVS-EOM-CCSD level of theory using the $^2DC^M$ and the $^2DCG^M$ Hamiltonians without contributions from the (SS|SS) integrals and the Dyall (D) basis set.

5. CONCLUSIONS

We have presented an implementation of the core−valence separation for the equation-of-motion coupled-cluster method in the DIRAC program. This implementation, which is based on a flexible framework for defining projection operators, enables the calculation of ionization and excitation energies for all four-component-based Hamiltonians available in DIRAC, and consequently for nonrelativistic Hamiltonians as well. We have applied our implementation to the calculation of core electron binding energies for halogen (CH_3I, X^-, and HX, X = Cl−At) and Xe species (Xe, XeF_2). For the latter, we also briefly explored the calculation of core excitations. With these systems, we have investigated the performance of different approximations to the original CVS approach, the basis set effects, and the performance of different classes of two-component approximations.

For highly symmetric species such as the lighter halides, for which we are able to exactly diagonalize the original similarity-transformed Hamiltonian, we show that the CVS energies closely match those from exact diagonalization at all edges. For the overall test set, our assessment of the different approximations indicates the one which more closely matches the performance of the original CVS scheme, which employs both frozen core and the removal of doubly excited determinants containing only core occupied spinors. Taken individually, these approximations yield sizeable overestimations and underestimations to the core-ionization energies, respectively.

https://doi.org/10.1021/acs.jctc.0c01203
J. Chem. Theory Comput. 2021, 17, 3583−3598

With respect to the Hamiltonians, we observe first that the calculations in which the transformation to two-component is performed after the SCF step ($^2DC^M$) are nearly indistinguishable from the equivalent four-component ones (^4DC), though non-negligible discrepancies appear at the K edge of fifth and sixth-row elements. We have traced these discrepancies to the use of the uncorrected 2-electron operator in the two-component molecular mean-field scheme ($^2DC^M$ and $^2DCG^M$). More approximate approaches in which the transformation to two-component is carried out before the SCF step (X2C-AMFI and X2C-G-AMFI), on the other hand, offer at best qualitative accuracy. Second, our results underscore the importance of explicitly considering SSSS-type integrals, in particular from the fifth row onwards.

A comparison to experimental results for Xe, XeF_2, and CH_3I underscores the importance of the QED, Breit, and higher-order correlation effects to approach the experimental results. While our calculations, including the Gaunt interaction, recover a significant fraction of the Breit interaction, the gauge term remains quite significant for the K and L edges, and it must be accounted for.

In view of these findings, we consider the four-component-based CVS-EOM-CCSD as a reliable approach for investigating core properties throughout the periodic table. Apart from its intrinsic interest, it may serve as a basis for further investigations of the reliability of more approximate schemes for atoms beyond the fifth row, as well as to verify whether such approximations result in significant changes for properties such as transition moments, that require the determination of the excited-state wave functions.

■ ASSOCIATED CONTENT

Supporting Information

The Supporting Information is available free of charge at https://pubs.acs.org/doi/10.1021/acs.jctc.0c01203.

Figures of the effect of the CVS variants on the different binding energies of Xe, the effect of the REW variants on the different binding energies of Cl^-, Br^-, I^-, HCl, HBr, and HI; table illustrating the operation count corresponding to the construction of the σ vector of the EOM-EE and EOM-IP equations using the dyall.acv3z basis set for Cl^- and At^-; and working equations for EOM-EE and EOM-IP σ vectors (PDF)

■ AUTHOR INFORMATION

Corresponding Authors

Loïc Halbert − *CNRS, UMR 8523—PhLAM—Physique des Lasers, Atomes et Molécules, Université de Lille, F-59000 Lille, France*; Email: loic.halbert@univ-lille.fr

Marta L. Vidal − *DTU Chemistry—Department of Chemistry, Technical University of Denmark, DK-2800 Kongens Lyngby, Denmark*; orcid.org/0000-0003-0653-2078; Email: malop@kemi.dtu.dk

Avijit Shee − *Department of Chemistry, University of Michigan, Ann Arbor, Michigan 48109, United States*; orcid.org/0000-0001-5042-3843; Email: ashee@umich.edu

Sonia Coriani − *DTU Chemistry—Department of Chemistry, Technical University of Denmark, DK-2800 Kongens Lyngby, Denmark*; orcid.org/0000-0002-4487-897X; Email: soco@kemi.dtu.dk

André Severo Pereira Gomes − *CNRS, UMR 8523—PhLAM—Physique des Lasers, Atomes et Molécules, Université de Lille, F-59000 Lille, France*; orcid.org/0000-0002-5437-2251; Email: andre.gomes@univ-lille.fr

Complete contact information is available at: https://pubs.acs.org/10.1021/acs.jctc.0c01203

Notes

The authors declare no competing financial interest.

■ ACKNOWLEDGMENTS

A.S.P.G. and L.H. acknowledge support from the PIA ANR project CaPPA (ANR-11-LABX-0005-01), the Franco-German project CompRIXS (Agence Nationale de la recherche ANR-19-CE29-0019, Deutsche Forschungsgemeinschaft JA 2329/6-1), I-SITE ULNE projects OVERSEE and MESONM International Associated Laboratory (LAI) (ANR-16-IDEX-0004), the French Ministry of Higher Education and Research, region Hauts de France council and European Regional Development Fund (ERDF) project CPER CLIMIBIO, and the French national supercomputing facilities (grants DARI A0050801859, A0070801859), as well as discussions with Trond Saue at the 2020 DIRAC Developers' meeting and following the appearance of the manuscript as a preprint. MLV and SC acknowledge support from DTU Chemistry (start-up Ph.D. grant), the Independent Research Fund Denmark−Natural Sciences, Research Project 2, grant no. 7014-00258B, and the European Union's Horizon 2020 research and innovation program under the Marie Skłodowska-Curie European Training Network COmputational Spectroscopy In Natural sciences and Engineering (COSINE), grant agreement no. 765739. Support from the COST action CM1405 MOLIM: Molecules in Motion (short-term mobility grant to M.L.V. to visit A.S.P.G.) is also acknowledged.

■ REFERENCES

(1) Stöhr, J. *NEXAFS Spectroscopy*; Springer: Berlin, 1992.

(2) Norman, P.; Dreuw, A. Simulating X-ray Spectroscopies and Calculating Core-Excited States of Molecules. *Chem. Rev.* **2018**, *118*, 7208−7248.

(3) *X-Ray Absorption and X-ray Emission Spectroscopy; Theory and Applications*; van Bokhoven, J.; Lamberti, C., Eds.; Wiley & Sons, 2016.

(4) *Synchrotron Radiation: Basics, Methods and Applications*; Mobilio, S.; Boscherini, F.; Meneghini, C., Eds.; Springer, 2014.

(5) *X-Ray Free Electron Lasers: Applications in Materials, Chemistry and Biology*; Bergmann, U.; Yachandra, V.; Yano, J., Eds.; Energy and Environment Series 18; Royal Society of Chemistry, 2017.

(6) Nisoli, M.; Decleva, P.; Calegari, F.; Palacios, A.; Martín, F. Attosecond Electron Dynamics in Molecules. *Chem. Rev.* **2017**, *117*, 10760−10825.

(7) Milne, C. J.; Penfold, T. J.; Chergui, M. Recent experimental and theoretical developments in time-resolved X-ray spectroscopies. *Coord. Chem. Rev.* **2014**, *277*−*278*, 44−68.

(8) Bagus, P. S. Self-Consistent-Field Wave Functions for Hole States of Some Ne-Like and Ar-Like Ions. *Phys. Rev.* **1965**, *139*, A619−A634.

(9) Bagus, P. S.; Schaefer, H. F. Direct Near-Hartree-Fock Calculations on the 1s Hole States of NO^+. *J. Chem. Phys.* **1971**, *55*, 1474−1475.

(10) Besley, N. A. Modeling of the spectroscopy of core electrons with density functional theory. *WIREs Comput. Mol. Sci.* **2021**, No. e1527.

(11) South, C.; Shee, A.; Mukherjee, D.; Wilson, A. K.; Saue, T. 4-Component relativistic calculations of L_3 ionization and excitations for the isoelectronic species UO_2^{2+}, OUN^+ and UN_2. *Phys. Chem. Chem. Phys.* **2016**, *18*, 21010−21023.

(12) Zheng, X.; Cheng, L. Performance of Delta-Coupled-Cluster Methods for Calculations of Core-Ionization Energies of First-Row Elements. *J. Chem. Theory Comput.* **2019**, *15*, 4945−4955.

(13) Lee, J.; Small, D. W.; Head-Gordon, M. Excited states via coupled cluster theory without equation-of-motion methods: Seeking higher roots with application to doubly excited states and double core hole states. *J. Chem. Phys.* **2019**, *151*, No. 214103.
(14) Besley, N. A.; Gilbert, A. T. B.; Gill, P. M. W. Self-consistent-field calculations of core excited states. *J. Chem. Phys.* **2009**, *130*, No. 124308.
(15) Liang, Y.; Vinson, J.; Pemmaraju, S.; Drisdell, W. S.; Shirley, E. L.; Prendergast, D. Accurate X-Ray Spectral Predictions: An Advanced Self-Consistent-Field Approach Inspired by Many-Body Perturbation Theory. *Phys. Rev. Lett.* **2017**, *118*, No. 096402.
(16) Hait, D.; Head-Gordon, M. Highly Accurate Prediction of Core Spectra of Molecules at Density Functional Theory Cost: Attaining Sub-electronvolt Error from a Restricted Open-Shell Kohn—Sham Approach. *J. Phys. Chem. Lett.* **2020**, *11*, 775−786.
(17) Ehlert, C.; Klamroth, T. PSIXAS: A Psi4 plugin for efficient simulations of X-ray absorption spectra based on the transition-potential and Δ-Kohn-Sham method. *J. Comput. Chem.* **2020**, *41*, 1781−1789.
(18) Derricotte, W. D.; Evangelista, F. A. Simulation of X-ray absorption spectra with orthogonality constrained density functional theory. *Phys. Chem. Chem. Phys.* **2015**, *17*, 14360−14374.
(19) Verma, P.; Derricotte, W. D.; Evangelista, F. A. Predicting Near Edge X-ray Absorption Spectra with the Spin-Free Exact-Two-Component Hamiltonian and Orthogonality Constrained Density Functional Theory. *J. Chem. Theory Comput.* **2016**, *12*, 144−156. PMID: 26584082.
(20) Hunt, s. J.; Goddard, W. A. Excited States of H_2O using improved virtual orbitals. *Chem. Phys. Lett.* **1969**, *3*, 414−418.
(21) Ågren, H.; Carravetta, V.; Vahtras, O.; Pettersson, L. G. M. Direct, atomic orbital, static exchange calculations of photoabsorption spectra of large molecules and clusters. *Chem. Phys. Lett.* **1994**, *222*, 75−81.
(22) Ferré, N.; Assfeld, X. Application of the local self-consistent-field method to core-ionized and core-excited molecules, polymers, and proteins: True orthogonality between ground and excited states. *J. Chem. Phys.* **2002**, *117*, 4119−4125.
(23) Lundberg, M.; Delcey, M. G. Multiconfigurational Approach to X-ray Spectroscopy of Transition Metal Complexes. In *Transition Metals in Coordination Environments: Computational Chemistry and Catalysis Viewpoints*; Broclawik, E.; Borowski, T.; Radoń, M., Eds.; Springer International Publishing: Cham, 2019; pp 185−217.
(24) Bokarev, S. I.; Kühn, O. Theoretical X-ray spectroscopy of transition metal compounds. *WIREs Comput. Mol. Sci.* **2020**, *10*, No. e1433.
(25) Klooster, R.; Broer, R.; Filatov, M. Calculation of X-ray photoelectron spectra with the use of the normalized elimination of the small component method. *Chem. Phys.* **2012**, *395*, 122−127.
(26) Maganas, D.; Kowalska, J. K.; Nooijen, M.; DeBeer, S.; Neese, F. Comparison of multireference ab initio wavefunction methodologies for X-ray absorption edges: A case study on $[Fe(II/III)Cl_4]^{2-/1-}$ molecules. *J. Chem. Phys.* **2019**, *150*, No. 104106.
(27) Coriani, S.; Christiansen, O.; Fransson, T.; Norman, P. Coupled-Cluster Response Theory for Near-Edge X-Ray-Absorption Fine Structure of Atoms and Molecules. *Phys. Rev. A* **2012**, *85*, No. 022507.
(28) Coriani, S.; Koch, H. Communication: X-ray Absorption Spectra and Core-Ionization Potentials within a Core-Valence Separated Coupled Cluster Framework. *J. Chem. Phys.* **2015**, *143*, No. 181103.
(29) Coriani, S.; Koch, H. Erratum: "Communication: X-ray absorption spectra and core-ionization potentials within a core-valence separated coupled cluster framework" [J. Chem. Phys. 143, 181103 (2015)]. *J. Chem. Phys.* **2016**, *145*, No. 149901.
(30) Sadybekov, A.; Krylov, A. I. Coupled-cluster based approach for core-ionized and core-excited states in condensed phase: Theory and application to different protonated forms of aqueous glycine. *J. Chem. Phys.* **2017**, *147*, No. 014107.
(31) Vidal, M. L.; Feng, X.; Epifanovsky, E.; Krylov, A. I.; Coriani, S. New and Efficient Equation-of-Motion Coupled-Cluster Framework for Core-Excited and Core-Ionized States. *J. Chem. Theory Comput.* **2019**, *15*, 3117−3133.
(32) Peng, B.; Lestrange, P. J.; Goings, J. J.; Caricato, M.; Li, X. Energy-Specific Equation-of-Motion Coupled-Cluster Methods for High-Energy Excited States: Application to K-Edge X-Ray Absorption Spectroscopy. *J. Chem. Theory Comput.* **2015**, *11*, 4146.
(33) Paul, A. C.; Myhre, R. H.; Koch, H. New and Efficient Implementation of CC3. *J. Chem. Theory Comput.* **2021**, *17*, 117−126. PMID: 33263255.
(34) Park, Y. C.; Perera, A.; Bartlett, R. J. Equation of motion coupled-cluster for core excitation spectra: Two complementary approaches. *J. Chem. Phys.* **2019**, *151*, No. 164117.
(35) Matthews, D. A. EOM-CC methods with approximate triple excitations applied to core excitation and ionisation energies. *Mol. Phys.* **2020**, *118*, No. e1771448.
(36) Brabec, J.; Bhaskaran-Nair, K.; Govind, N.; Pittner, J.; Kowalski, K. Communication: Application of state-specific multireference coupled cluster to core-level excitations. *J. Chem. Phys.* **2012**, *137*, No. 171101.
(37) Helmich-Paris, B. Simulating X-ray absorption spectra with complete active space self-consistent field linear response methods. *Int. J. Quantum Chem.* **2021**, *121*, No. e26559.
(38) Schirmer, J.; Thiel, A. An intermediate state representation approach to K-shell ionization in molecules. I. Theory. *J. Chem. Phys.* **2001**, *115*, No. 10621.
(39) Wenzel, J.; Wormit, M.; Dreuw, A. Calculating Core-Level Excitations and X-Ray Absorption Spectra of Medium-Sized Closed-Shell Molecules with the Algebraic-Diagrammatic Construction Scheme for the Polarization Propagator. *J. Comput. Chem.* **2014**, *35*, 1900.
(40) Dreuw, A.; Wormit, M. The algebraic diagrammatic construction scheme for the polarization propagator for the calculation of excited states. *WIREs Comput. Mol. Sci.* **2015**, *5*, 82−95.
(41) Neville, S. P.; Averbukh, V.; Patchkovskii, S.; Ruberti, M.; Yun, R.; Chergui, M.; Stolow, A.; Schuurman, M. S. Beyond structure: ultrafast X-ray absorption spectroscopy as a probe of non-adiabatic wavepacket dynamics. *Faraday Discuss.* **2016**, *194*, 117−145.
(42) Ekström, U.; Norman, P.; Carravetta, V.; Ågren, H. Polarization Propagator for X-Ray Spectra. *Phys. Rev. Lett.* **2006**, *97*, No. 143001.
(43) Besley, N. A. Density Functional Theory Based Methods for the Calculation of X-ray Spectroscopy. *Acc. Chem. Res.* **2020**, *53*, 1306−1315.
(44) Stanton, J.; Bartlett, R. The equation of motion coupled-cluster method. A systematic biorthogonal approach to molecular excitation energies, transition probabilities, and excited state properties. *J. Chem. Phys.* **1993**, *98*, 7029−7039.
(45) Sneskov, K.; Christiansen, O. Excited state coupled cluster methods. *WIREs Comput. Mol. Sci.* **2012**, *2*, 566−584.
(46) Bartlett, R. J. Coupled-cluster theory and its equation-of-motion extensions. *WIREs Comput. Mol. Sci.* **2012**, *2*, 126−138.
(47) Krylov, A. I. Equation-of-Motion Coupled-Cluster Methods for Open-Shell and Electronically Excited Species: The Hitchhiker's Guide to Fock Space. *Ann. Rev. Phys. Chem.* **2008**, *59*, 433−462.
(48) Christiansen, O.; Jørgensen, P.; Hättig, C. Response Functions from Fourier Component Variational Perturbation Theory Applied to a Time-Averaged Quasienergy. *Int. J. Quantum Chem.* **1998**, *98*, 1.
(49) Koch, H.; Jørgensen, P. Coupled Cluster Response Functions. *J. Chem. Phys.* **1990**, *93*, 3333−3344.
(50) Coriani, S.; Pawlowski, F.; Olsen, J.; Jørgensen, P. Molecular response properties in equation of motion coupled cluster theory: A time-dependent perspective. *J. Chem. Phys.* **2016**, *144*, No. 024102.
(51) Zuev, D.; Vecharynski, E.; Yang, C.; Orms, N.; Krylov, A. I. New algorithms for iterative matrix-free eigensolvers in quantum chemistry. *J. Comput. Chem.* **2015**, *36*, 273−284.
(52) Huang, C.; Liu, W.; Xiao, Y.; Hoffmann, M. R. iVI: An iterative vector interaction method for large eigenvalue problems. *J. Comput. Chem.* **2017**, *38*, 2481−2499.
(53) Huang, C.; Liu, W. iVI-TD-DFT: An iterative vector interaction method for exterior/interior roots of TD-DFT. *J. Comput. Chem.* **2019**, *40*, 1023−1037.

https://doi.org/10.1021/acs.jctc.0c01203
J. Chem. Theory Comput. 2021, 17, 3583−3598

(54) Stener, M.; Fronzoni, G.; de Simone, M. Time dependent density functional theory of core electrons excitations. *Chem. Phys. Lett.* **2003**, *373*, 115−123.
(55) Tenorio, B. N. C.; Moitra, T.; Nascimento, M. A. C.; Rocha, A. B.; Coriani, S. Molecular inner-shell photoabsorption/photoionization cross sections at core-valence-separated coupled cluster level: Theory and examples. *J. Chem. Phys.* **2019**, *150*, No. 224104.
(56) Seidu, I.; Neville, S. P.; Kleinschmidt, M.; Heil, A.; Marian, C. M.; Schuurman, M. S. The simulation of X-ray absorption spectra from ground and excited electronic states using core-valence separated DFT/MRCI. *J. Chem. Phys.* **2019**, *151*, No. 144104.
(57) Delcey, M. G.; Sørensen, L. K.; Vacher, M.; Couto, R. C.; Lundberg, M. Efficient calculations of a large number of highly excited states for multiconfigurational wavefunctions. *J. Comput. Chem.* **2019**, *40*, 1789−1799.
(58) Cederbaum, L. S.; Domcke, W.; Schirmer, J. Many-body theory of core holes. *Phys. Rev. A: At., Mol., Opt. Phys.* **1980**, *22*, 206−222.
(59) Faber, R.; Coriani, S. Core−valence-separated coupled-cluster-singles-and-doubles complex-polarization-propagator approach to X-ray spectroscopies. *Phys. Chem. Chem. Phys.* **2020**, *22*, 2642.
(60) Nanda, K. D.; Vidal, M. L.; Faber, R.; Coriani, S.; Krylov, A. I. How to stay out of trouble in RIXS calculations within the equation-of-motion coupled-cluster damped response theory framework? Safe hitchhiking in the excitation manifold by means of core-valence separation. *Phys. Chem. Chem. Phys.* **2020**, *22*, 2629.
(61) Dyall, K. G.; Faegri, K., Jr *Introduction to Relativistic Quantum Chemistry*; Oxford University Press, 2007.
(62) Saue, T. Relativistic Hamiltonians for Chemistry: A Primer. *ChemPhysChem* **2011**, *12*, 3077.
(63) Liu, W. Essentials of relativistic quantum chemistry. *J. Chem. Phys.* **2020**, *152*, No. 180901.
(64) Carbone, J. P.; Cheng, L.; Myhre, R. H.; Matthews, D.; Koch, H.; Coriani, S. Chapter Eleven - An Analysis of the Performance of Coupled Cluster Methods for K-edge Core Excitations and Ionizations using Standard Basis Sets. In *State of The Art of Molecular Electronic Structure Computations: Correlation Methods, Basis Sets and More*; Ancarani, L. U.; Hoggan, P. E., Eds.; Advances in Quantum Chemistry; Academic Press, 2019; Vol. *79*, pp 241−261.
(65) Liu, J.; Matthews, D.; Coriani, S.; Cheng, L. Benchmark Calculations of K-Edge Ionization Energies for First-Row Elements Using Scalar-Relativistic Core-Valence-Separated Equation-of-Motion Coupled-Cluster Methods. *J. Chem. Theory Comput.* **2019**, *15*, 1642−1651.
(66) Vidal, M. L.; Pokhilko, P.; Krylov, A. I.; Coriani, S. Equation-of-Motion Coupled-Cluster Theory to Model L-Edge X-ray Absorption and Photoelectron Spectra. *J. Phys. Chem. Lett.* **2020**, *11*, 8314−8321.
(67) Keller, L.; Blum, V.; Rinke, P.; Golze, D. Relativistic correction scheme for core-level binding energies from GW. *J. Chem. Phys.* **2020**, *153*, No. 114110.
(68) Fillaux, C.; Den Auwer, C.; Guillaumont, D.; Shuh, D. K.; Tyliszczak, T. Investigation of actinide compounds by coupling X-ray absorption spectroscopy and quantum chemistry. *J. Alloys Compd.* **2007**, *444*−*445*, 443−446.
(69) Bagus, P. S.; Ilton, E. S.; Nelin, C. J. The interpretation of XPS spectra: Insights into materials properties. *Surf. Sci. Rep.* **2013**, *68*, 273−304.
(70) Repisky, M.; Komorovsky, S.; Kadek, M.; Konecny, L.; Ekström, U.; Malkin, E.; Kaupp, M.; Ruud, K.; Malkina, O. L.; Malkin, V. G. ReSpect: Relativistic spectroscopy DFT program package. *J. Chem. Phys.* **2020**, *152*, No. 184101.
(71) Belpassi, L.; De Santis, M.; Quiney, H. M.; Tarantelli, F.; Storchi, L. BERTHA: Implementation of a four-component Dirac-Kohn-Sham relativistic framework. *J. Chem. Phys.* **2020**, *152*, No. 164118.
(72) Zhang, Y.; Suo, B.; Wang, Z.; Zhang, N.; Li, Z.; Lei, Y.; Zou, W.; Gao, J.; Peng, D.; Pu, Z.; Xiao, Y.; Sun, Q.; Wang, F.; Ma, Y.; Wang, X.; Guo, Y.; Liu, W. BDF: A relativistic electronic structure program package. *J. Chem. Phys.* **2020**, *152*, No. 064113.
(73) Kutzelnigg, W.; Liu, W. Quasirelativistic theory equivalent to fully relativistic theory. *J. Chem. Phys.* **2005**, *123*, No. 241102.
(74) Jensen, H. J. A. Douglas−Krollthe Easy Way. Talk at Conference on Relativistic Effects in Heavy Elements—REHE, Mülheim, Germany, April, 2005. Available at https://doi.org/10.6084/m9.figshare.12046158.
(75) Liu, W.; Peng, D. Infinite-order quasirelativistic density functional method based on the exact matrix quasirelativistic theory. *J. Chem. Phys.* **2006**, *125*, No. 044102.
(76) Iliaš, M.; Saue, T. An infinite-order two-component relativistic Hamiltonian by a simple one-step transformation. *J. Chem. Phys.* **2007**, *126*, No. 064102.
(77) Peng, D.; Liu, W.; Xiao, Y.; Cheng, L. Making four- and two-component relativistic density functional methods fully equivalent based on the idea of "from atoms to molecule". *J. Chem. Phys.* **2007**, *127*, No. 104106.
(78) Liu, W.; Peng, D. Exact two-component Hamiltonians revisited. *J. Chem. Phys.* **2009**, *131*, No. 031104.
(79) Sikkema, J.; Visscher, L.; Saue, T.; Iliaš, M. The molecular mean-field approach for correlated relativistic calculations. *J. Chem. Phys.* **2009**, *131*, No. 124116.
(80) Liu, J.; Shen, Y.; Asthana, A.; Cheng, L. Two-component relativistic coupled-cluster methods using mean-field spin-orbit integrals. *J. Chem. Phys.* **2018**, *148*, No. 034106.
(81) Liu, J.; Cheng, L. An atomic mean-field spin-orbit approach within exact two-component theory for a non-perturbative treatment of spin-orbit coupling. *J. Chem. Phys.* **2018**, *148*, No. 144108.
(82) Cheng, L. A study of non-iterative triples contributions in relativistic equation-of-motion coupled-cluster calculations using an exact two-component Hamiltonian with atomic mean-field spin-orbit integrals: Application to uranyl and other heavy-element compounds. *J. Chem. Phys.* **2019**, *151*, No. 104103.
(83) Asthana, A.; Liu, J.; Cheng, L. Exact two-component equation-of-motion coupled-cluster singles and doubles method using atomic mean-field spin-orbit integrals. *J. Chem. Phys.* **2019**, *150*, No. 074102.
(84) Shee, A.; Saue, T.; Visscher, L.; S.P.Gomes, A. Equation-of-motion coupled-cluster theory based on the 4-component Dirac-Coulomb (-Gaunt) Hamiltonian. Energies for single electron detachment, attachment, and electronically excited states. *J. Chem. Phys.* **2018**, *149*, No. 174113.
(85) Saue, T.; Bast, R.; Gomes, A. S. P.; Jensen, H. J. A.; Visscher, L.; Aucar, I. A.; Di Remigio, R.; Dyall, K. G.; Eliav, E.; Fasshauer, E.; Fleig, T.; Halbert, L.; Hedegård, E. D.; Helmich-Paris, B.; Iliaš, M.; Jacob, C. R.; Knecht, S.; Laerdahl, J. K.; Vidal, M. L.; Nayak, M. K.; Olejniczak, M.; Olsen, J. M. H.; Pernpointner, M.; Senjean, B.; Shee, A.; Sunaga, A.; van Stralen, J. N. P. The DIRAC code for relativistic molecular calculations. *J. Chem. Phys.* **2020**, *152*, No. 204104.
(86) Pathak, H.; Sasmal, S.; Nayak, M. K.; Vaval, N.; Pal, S. Relativistic equation-of-motion coupled-cluster method for the electron attachment problem. *Comput. Theor. Chem.* **2016**, *1076*, 94−100.
(87) Pathak, H.; Sahoo, B. K.; Sengupta, T.; Das, B. P.; Vaval, N.; Pal, S. A relativistic equation-of-motion coupled-cluster investigation of the trends of single and double ionization potentials in the He and Be isoelectronic systems. *J. Phys. B: At., Mol. Opt. Phys.* **2015**, *48*, 115009−115010.
(88) Pathak, H.; Sasmal, S.; Nayak, M. K.; Vaval, N.; Pal, S. Relativistic equation-of-motion coupled-cluster method for the ionization problem: Application to molecules. *Phys. Rev. A* **2014**, *90*, 062501−062507.
(89) Pathak, H.; Sahoo, B. K.; Das, B. P.; Vaval, N.; Pal, S. Relativistic equation-of-motion coupled-cluster method: Application to closed-shell atomic systems. *Phys. Rev. A* **2014**, *89*, 042510−042517.
(90) Pathak, H.; Sasmal, S.; Nayak, M. K.; Vaval, N.; Pal, S. Relativistic equation-of-motion coupled-cluster method using open-shell reference wavefunction: Application to ionization potential. *J. Chem. Phys.* **2016**, *145*, 074110−074118.
(91) Klein, K.; Gauss, J. Perturbative calculation of spin-orbit splittings using the equation-of-motion ionization-potential coupled-cluster ansatz. *J. Chem. Phys.* **2008**, *129*, 194106−194107.

(92) Yang, D.-D.; Wang, F.; Guo, J. Equation of motion coupled cluster method for electron attached states with spin-orbit coupling. *Chem. Phys. Lett.* **2012**, *531*, 236−241.
(93) Wang, Z.; Hu, S.; Wang, F.; Guo, J. Equation-of-motion coupled-cluster method for doubly ionized states with spin-orbit coupling. *J. Chem. Phys.* **2015**, *142*, 144109−144110.
(94) Epifanovsky, E.; Klein, K.; Stopkowicz, S.; Gauss, J.; Krylov, A. I. Spin-orbit couplings within the equation-of-motion coupled-cluster framework: Theory, implementation, and benchmark calculations. *J. Chem. Phys.* **2015**, *143*, 064102−064117.
(95) Cao, Z.; Wang, F.; Yang, M. Spin-orbit coupling with approximate equation-of-motion coupled-cluster method for ionization potential and electron attachment. *J. Chem. Phys.* **2016**, *145*, 154110−154113.
(96) Cao, Z.; Li, Z.; Wang, F.; Liu, W. Combining spin-separated exact two-component relativistic Hamiltonian with equation-of-motion coupled-cluster for spin-orbit splittings of light and heavy elements. *Phys. Chem. Chem. Phys.* **2017**, *19*, 3713−3721.
(97) Zhang, S.; Wang, F. Excitation Energies of UO_2^{2+}, NUO^+, and NUN Based on Equation-of-Motion Coupled-Cluster Theory with Spin−Orbit Coupling. *J. Phys. Chem. A* **2017**, *121*, 3966−3975.
(98) Akinaga, Y.; Nakajima, T. Two-Component Relativistic Equation-of-Motion Coupled-Cluster Methods for Excitation Energies and Ionization Potentials of Atoms and Molecules. *J. Phys. Chem. A* **2017**, *121*, 827−835.
(99) Wang, F. Relativistic Equation-of-Motion Coupled-Cluster Theory (EOM-CC). In *Handbook of Relativistic Quantum Chemistry*; Liu, W., Ed.; Springer: Berlin, 2016; pp 1−27.
(100) Guo, M.; Wang, Z.; Wang, F. Equation-of-motion coupled-cluster theory for double electron attachment with spin−orbit coupling. *J. Chem. Phys.* **2020**, *153*, No. 214118.
(101) Pathak, H.; Sasmal, S.; Talukdar, K.; Nayak, M. K.; Vaval, N.; Pal, S. Relativistic double-ionization equation-of-motion coupled-cluster method: Application to low-lying doubly ionized states. *J. Chem. Phys.* **2020**, *152*, No. 104302.
(102) Folkestad, S. D.; Kjønstad, E. F.; Myhre, R. H.; Andersen, J. H.; Balbi, A.; Coriani, S.; Giovannini, T.; Goletto, L.; Haugland, T. S.; Hutcheson, A.; Høyvik, I.-M.; Moitra, T.; Paul, A. C.; Scavino, M.; Skeidsvoll, A. S.; Tveten, Å. H.; Koch, H. eT 1.0: An open source electronic structure program with emphasis on coupled cluster and multilevel methods. *J. Chem. Phys.* **2020**, *152*, No. 184103.
(103) Sorensen, S. L.; Zheng, X.; Southworth, S. H.; Patanen, M.; Kokkonen, E.; Oostenrijk, B.; Travnikova, O.; Marchenko, T.; Simon, M.; Bostedt, C.; Doumy, G.; Cheng, L.; Young, L. From synchrotrons for XFELs: the soft x-ray near-edge spectrum of the ESCA molecule. *J. Phys. B: At., Mol. Opt. Phys.* **2020**, *53*, No. 244011.
(104) Rankine, C. D.; Penfold, T. J.Progress in the Theory of X-ray Spectroscopy: From Quantum Chemistry to Machine Learning and Ultrafast Dynamics *J. Phys. Chem. A* PMID: 33729774; DOI: 10.1021/acs.jpca.0c11267.
(105) Wenzel, J.; Holzer, A.; Wormit, M.; Dreuw, A. Analysis and Comparison of CVS-ADC Approaches up to Third Order for the Calculation of Core-Excited States. *J. Chem. Phys.* **2015**, *142*, No. 214104.
(106) Visscher, L.; Lee, T. J.; Dyall, K. G. Formulation and implementation of a relativistic unrestricted coupled-cluster method including noniterative connected triples. *J. Chem. Phys.* **1996**, *105*, 8769−8776.
(107) Pernpointner, M.; Visscher, L. Parallelization of four-component calculations. II. Symmetry-driven parallelization of the 4-Spinor CCSD algorithm. *J. Comput. Chem.* **2003**, *24*, 754−759.
(108) Shee, A.; Visscher, L.; Saue, T. Analytic Gradient at the 4-component Relativistic Coupled Cluster Level with Inclusion of Spin-Orbit Coupling. *J. Chem. Phys.* **2016**, *145*, No. 184107.
(109) DIRAC, a relativistic ab initio electronic structure program, Release DIRAC19 (2009) written by Gomes, A. S. P.; Saue, T.; Visscher, L.; Aa, H. J.; Jensen, H. J. A.; Bast, R.; Aucar, I. A.; Bakken, V.; Dyall, K. G.; Dubillard, S.; Ekström, U.; Eliav, E.; Enevoldsen, T.; Faßhauer, E.; Fleig, T.; Fossgaard, O.; Halbert, L.; HedegÅrd, E. D.; Heimlich-Paris, B.; Helgaker, T.; Henriksson, J.; Iliaš, M.; Jacob, ChR.; Knecht, S.; Komorovský, S.; Kullie, O.; Lærdahl, J. K.; Larsen, C. V.; Lee, Y. S.; Nataraj, H. S.; Nayak, M. K.; Norman, P.; Olejniczak, G.; Olsen, J.; Olsen, J. M. H.; Park, Y. C.; Pedersen, J. K.; Pernpointner, M.; di Remigio, R.; Ruud, K.; Sałek, P.; Schimmelpfennig, B.; Senjean, B.; Shee, A.; Sikkema, J.; Thorvaldsen, A. J.; Thyssen, J.; van Stralen, J.; Vidal, M. L.; Villaume, S.; Visser, O.; Winther, T.; Yamamoto, S., written by (available at http://dx.doi.org/10.5281/zenodo.3572669, see also http://www.diracprogram.org).
(110) Dyall, K. G. Relativistic and nonrelativistic finite nucleus optimized triple-zeta basis sets for the 4p, 5p and 6p elements. *Theor. Chem. Acc.* **2002**, *108*, 335−340.
(111) Dyall, K. G. Relativistic and nonrelativistic finite nucleus optimized triple zeta basis sets for the 4p, 5p and 6p elements. *Theor. Chem. Acc.* **2003**, *109*, 284.
(112) Dyall, K. G. Relativistic double-zeta, triple-zeta, and quadruple-zeta basis sets for the light elements H-Ar. *Theor. Chem. Acc.* **2016**, *135*, No. 128.
(113) Roos, B. O.; Lindh, R.; Malmqvist, P.-A.; Veryazov, V.; Widmark, P.-O. Main Group Atoms and Dimers Studied with a New Relativistic ANO Basis Set. *J. Phys. Chem. A* **2004**, *108*, 2851−2858.
(114) Furry, W. H. On Bound States and Scattering in Positron Theory. *Phys. Rev.* **1951**, *81*, 115−124.
(115) Hess, B. A.; Marian, C. M.; Wahlgren, U.; Gropen, O. A mean-field spin-orbit method applicable to correlated wavefunctions. *Chem. Phys. Lett.* **1996**, *251*, 365−371.
(116) Marian, C. M. Spin-Orbit Coupling in Molecules. *Reviews in Computational Chemistry*; Wiley-VCH, 2001; Vol. *17*, p 99.
(117) Schimmelpfennig, B. *AMFI, An Atomic Mean-field Spin-Orbit Integral Program*; University of Stockholm: Stockholm, Sweden, 1999.
(118) Visscher, L. Approximate molecular relativistic Dirac-Coulomb calculations using a simple Coulombic correction. *Theor. Chem. Acc.* **1997**, *98*, 68−70.
(119) Cheng, L.; Gauss, J.; Stanton, J. F. Treatment of scalar-relativistic effects on nuclear magnetic shieldings using a spin-free exact-two-component approach. *J. Chem. Phys.* **2013**, *139*, No. 054105.
(120) *Structure of Free Polyatomic Molecules*; Kuchitsu, K., Ed.; Springer: Berlin, 1998.
(121) Visscher, L.; Styszyñski, J.; Nieuwpoort, W. C. Relativistic and correlation effects on molecular properties. II. The hydrogen halides HF, HCl, HBr, HI, and HAt. *J. Chem. Phys.* **1996**, *105*, 1987−1994.
(122) Halbert, L.; Vidal, M. L.; Shee, A.; Coriani, S.; Gomes, A. S. P. *Dataset: Relativistic EOM-CCSD for core-excited and core-ionized state energies based on the 4-component Dirac-Coulomb(-Gaunt) Hamiltonian* 2020; https://doi.org/10.5281/zenodo.4116366.
(123) Sarangi, R.; Vidal, M. L.; Coriani, S.; Krylov, A. I. On the basis set selection for calculations of core-level states: different strategies to balance cost and accuracy. *Mol. Phys.* **2020**, *118*, No. e1769872.
(124) Herbst, M. F.; Fransson, T. Quantifying the error of the core-valence separation approximation. *J. Chem. Phys.* **2020**, *153*, No. 054114.
(125) Kozioł, K.; Aucar, G. A. QED effects on individual atomic orbital energies. *J. Chem. Phys.* **2018**, *148*, No. 134101.
(126) Southworth, S. H.; Dunford, R. W.; Ray, D.; Kanter, E. P.; Doumy, G.; March, A. M.; Ho, P. J.; Krässig, B.; Gao, Y.; Lehmann, C. S.; Picón, A.; Young, L.; Walko, D. A.; Cheng, L. Observing pre-edge K-shell resonances in Kr, Xe, and XeF_2. *Phys. Rev. A* **2019**, *100*, No. 022507.
(127) Southworth, S. H.; Wehlitz, R.; Picón, A.; Lehmann, C. S.; Cheng, L.; Stanton, J. F. Inner-shell photoionization and core-hole decay of Xe and XeF_2. *J. Chem. Phys.* **2015**, *142*, No. 224302.
(128) Oura, M.; Gejo, T.; Nagaya, K.; Kohmura, Y.; Tamasaku, K.; Journel, L.; Piancastelli, M. N.; Simon, M. Hard x-ray photoelectron spectroscopy on heavy atoms and heavy-element containing molecules using synchrotron radiation up to 35 keV at SPring-8 undulator beamlines. *New J. Phys.* **2019**, *21*, No. 043015.
(129) Carroll, T. X.; Shaw, R. W., Jr.; Thomas, T. D.; Kindle, C.; Bartlett, N. Electron distribution in the xenon fluorides and xenon oxide

tetrafluoride by ESCA and evidence for orbital independence in the xenon-fluorine bonding. *J. Am. Chem. Soc.* **1974**, *96*, 1989−1996.
(130) Boudjemia, N.; Jänkälä, K.; Gejo, T.; Nagaya, K.; Tamasaku, K.; Huttula, M.; Piancastelli, M. N.; Simon, M.; Oura, M. Deep core photoionization of iodine in CH_3I and CF_3I molecules: how deep down does the chemical shift reach? *Phys. Chem. Chem. Phys.* **2019**, *21*, 5448−5454.
(131) Mooney, T.; Lindroth, E.; Indelicato, P.; Kessler, E. G.; Deslattes, R. D. Precision measurements of K and L transitions in xenon: Experiment and theory for the K, L, and M levels. *Phys. Rev. A* **1992**, *45*, 1531−1543.

https://doi.org/10.1021/acs.jctc.0c01203
J. Chem. Theory Comput. 2021, 17, 3583−3598